ISTANBUL TECHNICAL UNIVERSITY ⋆ INSTITUTE OF SCIENCE AND TECHNOLOGY

EFFECTS OF THE NON-AXISYMMETRIC PERTURBATIONS ON THE DIVERTOR TOKAMAKS

M.Sc. THESIS

Cuma YARIM , B.Sc.

Date of Submission : June 13, 1994

Date of Approval : June 30, 1994

Supervisor : Prof. Dr. Umur DAYBELGE

Member : Prof. Dr. Vural CINEMRE

Member : Prof. Dr. Avadis HACINLIYAN

JUNE 1994

İSTANBUL TEKNİK ÜNİVERSİTESİ ★ FEN BİLİMLERİ ENSTİTÜSÜ

EKSENEL SİMETRİK OLMAYAN TEDİRGENİMLERİN DİVERTOR TOKAMAKLARI ÜZERİNDEKİ ETKİLERİ

YÜKSEK LİSANS TEZİ

Müh. Cuma YARIM

Tezin Enstitüye Verildiği Tarih : 13 Haziran 1994

Tezin Savunulduğu Tarih : 30 Haziran 1994

Tez Danışmanı : Prof. Dr. Umur DAYBELGE

Diğer Jüri Üyeleri : Prof. Dr. Vural CİNEMRE

Prof. Dr. Avadis HACINLIYAN

HAZİRAN 1994

ACKNOWLEDGEMENTS

Energy generation is one of the great problem of our world, and naturally the need for energy will grow in the next century. To reach the endless energy source buried in the sea water is one of the solutions of this great problem of humanity, perhaps, with a great probability, the unique one. The source of the all phenomena in the universe, the source of the life on the earth, i.e. the fusion energy is also a way for reaching to the great dream of mankind, going to the planets of our solar system and to the near stars.

My thanks are due to my supervisor Prof. Dr. Umur DAYBELGE for leading me to this interesting subject; subject of yesterday, today and perhaps tomorrows. I appreciate his precious guidance and help throughout the study. With his efforts for this study, i can hardly use the adjective "MY" for this thesis.

All my labour made for this study is dedicated to Devrim, my only way. I would like to thank my friends at I.T.U., Faculty of Aeronautics and Astronautics, for their helps in every stage of this study. Thanks are also for the faculty administration for providing me, as a research assistant, the required working and studying conditions(!).

Cuma YARIM,

January 1994, İSTANBUL

CONTENTS

SUMMARY

It is strongly expected that energy consumption of humanity will considerably increase in the next century. The unique long–term solution is to supply fusion energy. The scientists have long tried to obtain energy from the fusion reaction. As a magnetic confinement device in toroidal form, tokamak is one of the experimentally fusion energy production devices, which is widely used. Divertors are used to get cleaner plasma in such devices.

In this study, particle motions in a double–null poloidal type divertor tokamak was investigated numerically. Three approach was used. In the first two, the drift motions are neglected, i.e., it is assumed that particles moves along the magnetic field lines. First one is based on modelling tokamak magnetic field by three, infinitely long, straight wires each carrying codirectional currents, two for divertors and the middle for the plasma itself. The second one uses more realistic current geometry; three circular wires. Both of the magnetic fields consist $n = 1$ mode perturbations to simulate the nonaxisymmetries due to the plasma instabilities and the imperfect construction of the field coils. At the last approach, the true particle motion is taken into account under the influence of the magnetic fields used as second approach.

Broadening of the magnetic separatrix, both chaotic and coherent structures in magnetic field lines and in particle orbits are observed in three approach by using Poincaré sections. Adams–Moulton numerical integration technique was used in calculations. It has been seen that, to see the real effect of nonaxisymmetry on the particle motions and to investigate heat deposition on the divertor plates, one should consider full particle equations, since the other approximations gives quiet different phase portraits. The next stages of this study will be the investigation of the effect of a transversal electric field on the particle drift orbits.

ÖZET

EKSENEL SİMETRİK OLMAYAN TEDİRGENİMLERİN DİVERTOR TOKAMAKLARI ÜZERİNDEKİ ETKİLERİ

Bu çalışmada, önümüzdeki yüzyılda üzerinde yoğun olarak çalışılacağı kesinleşen füzyon enerjisi elde etme araçlarından biri olan tokamak cihazlarıyla ilgilenilmiştir. Füzyon tepkimesini gerçekleştiren plazmanın, manyetik alanlar yardımıyla tutulduğu toroidal şekilli bu araçları aynı biçimli diğer araçlardan ayıran özellik, plazmanın içerisinden bir akım geçirilerek ek manyetik alan bileşenlerinin yaratılmasıdır. Böylece plazma daha uzun bir süre kararlı bir biçimde tutulabilmektedir.

Plazmayı uzun süre kararlı biçimde tutamamak, füzyon enerjisinin kısa sürede insanlığın hizmetine sunulabilmesini engelleyen sorunlardan birisidir. Bir diğer sorun ise, füzyon ürünü yüksek enerjili parçacıkların plazmayı çevreleyen kaba çarparak buradan ağır tanecikler koparmalarıdır. Ağır taneciklerin, hidrojen ve benzeri gibi hafif çekirdeklerin füzyon yaptıkları sıcaklık düzeylerinde aynı tepkimeyi vermeleri olanaksızdır. Dolayısıyla bu tanecikler, füzyon yapabilecek olan parçacıklara aktarılmak istenen enerjinin bir bölümünü almakta ve bu enerjiyi dışarıya ışınım yoluyla atarak plazmanın, füzyon için gerekli sıcaklık düzeyine kadar ısınmasını önlemektedirler. Tokamak cihazlarında kirlenmeyi azaltmak için divertor adı verilen akımlardan yararlanılır. Bu akımlar, plazmayı çevreleyen manyetik alan çizgilerini saptırarak divertor plakası adı verilen plakalara doğru yönlendirirler. Ağır tanecikler henüz plazmaya karışma olanağı bulamadan bu çizgileri izleyerek plakalara taşınırlar ve burada tutularak bir pompa ile emilirler.

Divertor akımlarının yakın civarında bulunan manyetik alan çizgileri bölgesiyle plazma civarındaki manyetik alan çizgileri bölgesini birbirinden ayıran yüzeye separatriks denir. Separatriksin tekil noktaları ise, bu nokta civarındaki alan geometrisi X harfine benzediğinden kimi zaman X–noktası, bu noktadaki manyetik alan değeri sıfır olduğundan dolayı da kimi zaman O–noktası olarak adlandırılırlar. Değişik tipte divertor akımlı tokamak cihazları vardır. Bu çalışmada çift poloidal divertorlü tokamak cihazları ele alınmış ve bunlardaki tanecik hareketleri incelenmiştir.

Tokamak cihazlarında kullanılan manyetik alanlar, gerek plazma içi kararsızlıklar ve gerekse bu manyetik alanları oluşturmak için kullanılan elektromıknatısların yerleştirilmelerinde yapılan hatalar nedeniyle eksenel simetriden saparlar. Bu çalışmada eksenel simetrik olmayan bu tedirgenimlerin divertor tokamaklarındaki etkileri incelenmiştir.

Bu amaçla yapılan ilk yaklaşımda taneciklerin manyetik alan çizgileri boyunca hareket ettikleri varsayılmıştır. Dolayısıyla, ilk yaklaşımda gerçek tanecik hareketleri yerine yalnızca manyetik alanları incelemek yeterli görülmüştür. Tokamak cihazının manyetik alanı, içlerinden aynı yönde akım geçen, üç, sonsuz uzunluklu düz telin manyetik alanıyla temsil edilmiştir.

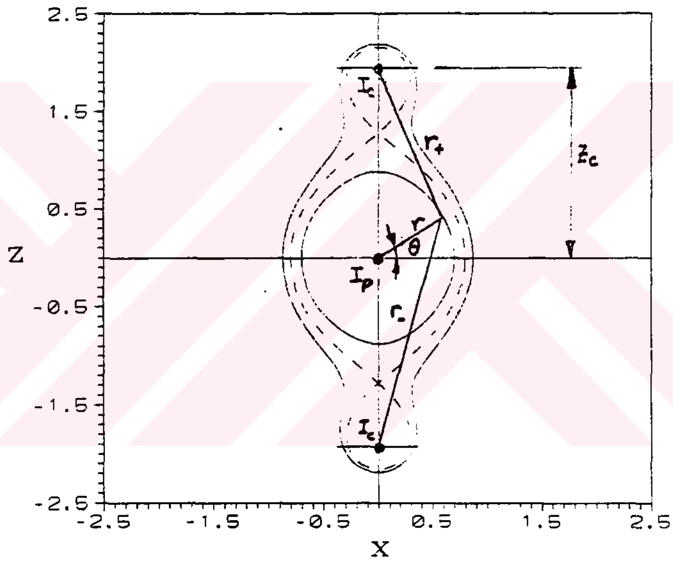

Şekil 1. İlk yaklaşım için akım geometrisi.

Şekil 1 de görülen bu akım geometrisi için, tedirgenimlerin olmadığı durumda manyetik alan denklemleri

$$\vec{B} = B_0 \hat{e}_\phi + \nabla \times \vec{A}_\phi \quad (1)$$

biçiminde verilir. Burada $\vec{A}_\phi = \hat{e}_\phi \Psi(x, z)$, $\Psi = B_0 L \log(r_+^{2\gamma} r^2 r_-^{2\gamma})$ ve $r_\mp^2 = z_c^2 + r^2 \mp 2 r z_c \cos\theta$ dır.

$n = 1$ modlu eksenel simetrik olmayan tedirgenimler için denklemlere $\delta\vec{B} = \nabla \times \delta\vec{A}$ eklenmiştir. $\delta\vec{A} = \hat{e}_z \varepsilon R_0 \exp(\frac{x}{R_0}) \cos\phi$ dir. Burada $\hat{e}_z$ büyük eksene paralel birim vektör, ϕ ise toroidal açı değeridir.

Alan çizgisi denklemleri

$$\frac{dx}{d\phi} = \frac{B_x}{B_\phi} \quad ; \quad \frac{dz}{d\phi} = \frac{B_z}{B_\phi} \tag{2}$$

ile, manyetik alan bileşenleri ise

$$B_x = \frac{\partial \Psi_0}{\partial z} + \varepsilon exp(\frac{x}{R_0}) \cos(\phi) \tag{3.a}$$

$$B_\phi = \frac{1}{R_0} \left[B_0 - \varepsilon \exp(\frac{x}{R_0}) \sin(\phi) \right] \tag{3.b}$$

$$B_z = -\frac{\partial \Psi_0}{\partial x} \tag{3.c}$$

denklemleri ile verilirler. Sayısal hesaplar için $\gamma = 0.64$; $z_c = 1.93$; uzunluk ölçeği $L = 0.06$; $R_0 = 2.67$, tedirgenim genliği $\varepsilon / B_0 = 0.001$ seçilmiştir. Sayısal integrasyon yöntemi olarak Adams-Moulton yöntemi kullanılmıştır.

Manyetik alan çizgilerinin dinamiği, biri, divertor plakalarının yerleştirilebileceği $z = -1.4$ düzlemine diğeri, $\phi = 0$ düzlemine yerleştirilmiş iki Poincaré kesidiyle görüntülenmiştir. Seçilen pertürbasyon değerinde, X noktasının yakın civarından kalkan yörüngelerin hem kaotik hem de kararlı yapılar oluşturdukları gözlenmiştir. Tedirgenim genliğinin artan değerlerinde kaotik bölge içine yuvalanmış olan kararlı yapıların küçülerek yok oldukları ve separatriks kalınlığının arttığı görülmüştür.

İkinci yaklaşım, ilk yaklaşımda düz olarak alınan tellerin, daha gerçekçi bir biçimde yuvarlak alınmasıyla yapılmıştır. Bu aşamada da taneciklerin sürüklenme hareketleri ihmal edilmiş ve yalnızca manyetik alan denklemleriyle yetinilmiştir.

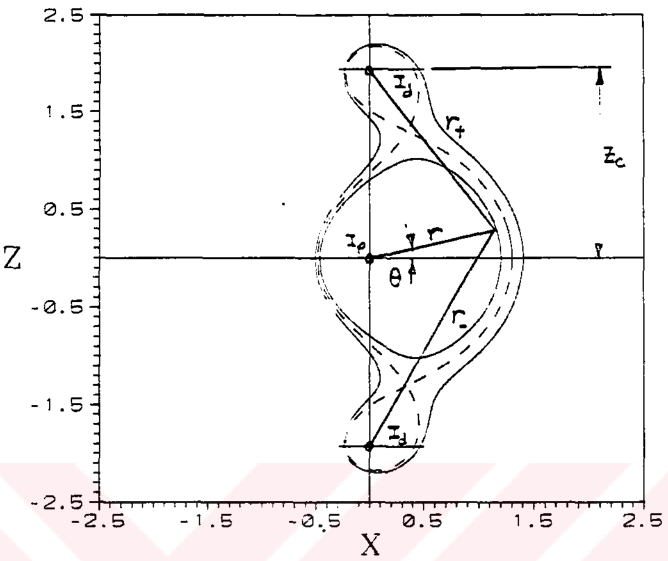

Şekil 2. İkinci yaklaşım için akım geometrisi.

Şekil 2. de verilen geometri için tedirgenim eklenmemiş manyetik alan denklemleri şöyledir:

$$\vec{B} = B_0\frac{\hat{\phi}}{h} + (B_x^p + B_x^+ + B_x^-)\hat{x} + (B_z^p + B_z^+ + B_z^-)\hat{z} \qquad (4)$$

burada $x = R - R_0$, $h = R/R_0 = 1 + (x/R_0)$. $+$, $-$ ve p üst indisleri, sırasıyla, $z = +z_d$, $z = -z_d$ ve $z = 0$ koordinatlarına yerleştirilmiş olan tellerin alan bileşenlerini, gösterir. $z = 0$ daki tel, ilk yaklaşımdaki gibi plazmanın kendisini temsil etmektedir. Manyetik alan bileşenleri

$$\begin{aligned} B_x &= I\frac{\mu_0}{4\pi}\frac{2\zeta}{\sqrt{(\rho+\rho_0)^2+\zeta^2}}\left[K(k) + \frac{1-k^2/2}{1-k^2}E(k)\right], \\ B_z &= I\frac{\mu_0}{4\pi}\frac{2}{\sqrt{(\rho+\rho_0)^2+\zeta^2}}\left[K(k) + \frac{\rho_0^2-\rho^2-\zeta^2}{(\rho_0+\rho)^2+\zeta^2}E(k)\right] \end{aligned} \qquad (5)$$

biçimindedirler. Burada

$$k^2 = \frac{4\rho_0\rho}{(\rho_0+\rho)^2+\zeta^2} \tag{6}$$

olarak alınır. Manyetik alanın poloidal kısmı

$$\vec{B} = \nabla \times \vec{A}_\phi \tag{7}$$

şeklinde verilen vektör potansiyeli ile tanımlanır. Burada

$$A_\phi = I\frac{\mu_0}{\pi k}\sqrt{\frac{\rho_0}{\rho}}\left[\left(1-\frac{k^2}{2}\right)K(k) - E(k)\right] \tag{8}$$

K ve E, sırasıyla birinci ve ikinci tipten tam eliptik integrallerdir.

B_p	için	:	$I = I_p$	;	$\rho_0 = R_0$	;	$\rho = R_0 + x$	;	$\zeta = z$
$B_\pm$	için	:	$I = I_d$	;	$\rho_0 = R_0 + x_d$	;	$\rho = R_0 + x$	;	$\zeta = z - (\pm z_d)$

alınır. Uzunluk skalası $\lambda = \dfrac{\mu_0 I_p}{4\pi R_0 B_0} = \dfrac{1}{qR_0}$ dır. Burada q güvenlik katsayısıdır.

Yukarıda tanımlı parametreler için hesaplarda kullanılan değerler aşağıdadır:

$$x_d = 0\ ;\quad z_d = 1.93\ ;\quad \gamma = I_d/I_p = 0.64\ ;\quad R_0 = 1/\varepsilon\ ;\quad \varepsilon = 0.3\ ;\quad \lambda = 0.06\varepsilon$$

Yukarıdaki eksenel simetrik poloidal manyetik alana eklenen $n = 1$ modlu tedirgenim terimleri şöyle verilmişlerdir:

$$\begin{aligned} \delta B_x &= \Theta\lambda B_0 \exp(x/R_0)\cos(\phi) \\ \delta B_\phi &= -\Theta\lambda B_0 \exp(x/R_0)\sin(\phi) \end{aligned} \tag{9}$$

Tedirgenim genliği miktarı $\Theta = 0.001/\lambda$ olarak seçilmiştir. Genişleyen separatriks ve bazı yörüngelerin kaotik davranışları her iki yaklaşımın ortak sonuçlarıdır. Poincaré kesidiyle görüntülenen faz uzaylarının her iki yaklaşımda çok farklı olması üç düz tel yaklaşımının yetersiz kaldığı sonucunu vermiştir.

Son olarak ikinci yaklaşımla verilen manyetik alan etkisi altındaki iyonların gerçek yörüngeleri izlenmiştir. Bir manyetik alandaki yüklü taneciğin hareketi; taneciğin, kılavuz merkez etrafındaki hızlı dönüşüyle kılavuz merkezin hareketinin süperpozisyonu ile temsil edilebilir. Bir manyetik alanda hareket eden yüklü bir taneciğin hareket denklemi

$$\frac{d\vec{x}}{dt} = v_{\parallel}\vec{b} + \frac{\vec{b}}{eB} \times \left[m v_{\parallel}^{2} \vec{b} \cdot \nabla \vec{b} + \mu_m \nabla B \right] \tag{10}$$

ile verilir. Burada $\mu_m = m v_{\parallel}^2/(2B)$ manyetik momenti, $\vec{b}$ ise manyetik alan vektörü yönündeki birim vektörü gösterirler. $v_{\parallel}$ ve $v_{\perp}$, sırasıyla, manyetik alan vektörüne paralel ve dik hızlardır. Tanecik yörüngeleri

$$\frac{dx}{dt} = F_x(x,z,\phi)\,; \quad \frac{dz}{dt} = F_z(x,z,\phi)\,; \quad \frac{d\phi}{dt} = F_\phi(x,z,\phi)\,; \tag{11}$$

ile gösterilebilecek denklem sisteminin integrasyonu ile elde edilebilirler. Tanecik yörüngeleri ile ikinci yaklaşımda verilen manyetik alan sonuçları karşılaştırıldığında, pozitif paralel hızlar için her iki dinamik sistem divertor plakasında benzer birer faz portresi verirlerken, negatif paralel hızlar için sistemlerin plakadaki portrelerinde önemli ölçüde farklılık olduğu görülmüştür. Buradan, yalnızca manyetik alanları kullanarak –yani sürüklenme hareketlerini ihmal ederek– yapılan yaklaşımın yeterince doğru sonuç vermediği ve parçacık dinamiği için parçacığın kendi denklemleriyle uğraşılması gerektiği sonucuna varılmıştır.

Çalışmanın bundan sonraki aşaması, genişleyen separatriks üzerine, bu bölgede homojen dağılmamış bir elektrik alanının parçacık dinamiği üzerine etkilerini incelemek ve buradan yola çıkarak bu elektrik alanının, tokamak cihazlarında rastlanılan; düşük moddan plazmanın daha iyi tutulabildiği yüksek moda geçişe olan etkisini incelemek olacaktır.

CHAPTER 1

INTRODUCTION

In this chapter, the question, 'Why to use fusion energy', will be tried to be answered from two point of views. The first will be about the possibility of travel in space, and the other, about the energy demand of mankind.

1.1 Fusion for Space Travel

Man has long dreamt of going to the other planets and to the nearest stars. Motivated by his unsatisfyable curiosity for knowing, this dream led him to reach the moon in 1969. This achievement, as his other ones, could not be enough for him but drive him to think of going to other stellar objects. However, the present propulsion systems based on the chemical reactions are not enough for this dream to come true. To put 1 extra kg to the earth orbit needs, approximately, 270 kg extra chemical fuel. This restriction makes it impossible to send the required amount of fuel for the interplanetary travel.

As a solution, Hohmann transfer orbits may be used for sending probes to distant stellar objects. In this method, which transfers a spacecraft from one orbit to another with minimum energy, i.e. with minimum fuel, the spacecraft is put into an intermediate elliptical orbit which at both ends of the major axis is tangent to the orbits around the two planetary objects. The main disadvantage of this orbit is the long travel time. An optimum case of rapid interplanetary space flight is one on which the shortest possible distance between two objects. During this flight, one may accelerate the probe with the uniform gravitational acceleration in the first half and decelerate it in the second half [1].

But a travel like this needs full powered flight and of course a lot of fuel. It is impossible to use chemical rockets to thrust the spacecraft on an optimal flight orbit. Full powered flight needs another kind of thrust method: Something with more energy and less fuel. The fusion is a kind of reaction which can supply the maximum energy per unit mass entering into the reaction.

Table 1.1 A comparison between two travelling method.

To	With Hohmann Ellipse	With Optimal Flight Path
Venus	147 days	35 hours
Mars	263 days	41 hours
Pluto	62 years	18 days

Although the research on fusion has been continuing for, about half of a century and it is thought to last another quarter of a century, it is not so much fictitious to compare such devices based on different systems. One of these has been submitted by Murthy and Froning [2]. In their study, the authors compare the effectiveness of nuclear and scramjet engines with respect to weights and utilization of energy availibility. In the suggested engine scheme, which can be seen in Figure 1.1, hydrogen is assumed to be heated in the pulsed *Deuterium* – *Helium*^{3} reactor.

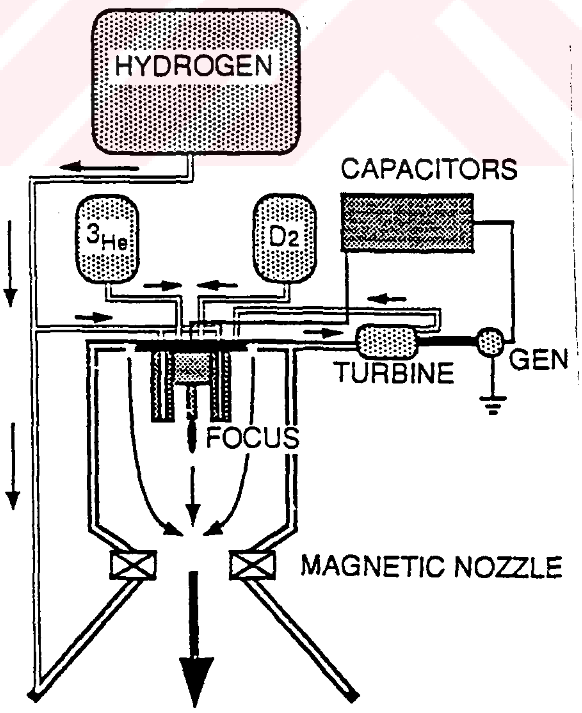

Figure 1.1 Schematic of dense plasma fusion engine.

The specific impulse based on consumption of hydrogen is assumed to be 1600–2400 secs, roughly 3.5–5.0 fold increase compared to that conventional combustion rocket engine. In a combined chemical electrical–nuclear engine, it is possible to energize the working fluid of a rocket motor or an air–breathing engine by mixing with products of fusion reaction, and heat transfer between the working fluid and fusion reaction products. A comparison between classical chemical engines and combined ones is given in the Table 1.2.

Table 1.2 A comparison between chemical and combined propulsion system.

Airbreathing and Rocket Propulsion	Energy Management During Powered Phase of Ascent	Relative Vehicle Size	Relative Gross Weight
Chemical	Airbreathing up to Mach 8, Rocket until Orbital Speed is Reached		1.0
	Airbreathing during Entire Ascent, plus Rocket Augmentation at Low and High Speed		0.45
Combined: Chemical Electrical Nuclear	Airbreathing up to Mach 8, Rocket until Orbital Speed is Reached		0.21
	Airbreathing during Entire Ascent, plus Rocket Augmentation at Low and High Speed		0.18

(10,000 lb Payload to Polar Orbit)

The next step to a combined engine is the one using full fusion energy. Since the hydrogen is the main element of the universe and it can be found everywhere in the interstellar region, it will not be an important problem to supply fuel for a spacecraft using fusion energy. As a result, it can be concluded that the fusion energy is the unique kind of energy which will make the humanity be able to undertake long range space flights.

1.2 Fusion for Energy

From the industrial revolution up to now the consumption of energy has considerably increased and in the next century, the energy needs of modern societies is expected to increase even much more. This is due to that machines started to be substituted for human labour and that manufacturing switched from small numbers of hand–made products to mass production. After that technological development, the exponentially growing energy demand of humanity is shown in Table 1.3.

Table 1.3 Energy demand of man. ($1\ Q = 10^{21}\ \ Joules$)

0 – 1850	0.3–0.5	Q/century
1851 – 1950	4	Q/century
1951 – 2000	15	Q/half–century

Since the estimated world reserves of fossil fuels totally about 80 Q, ($1\ Q = 10^{21}\ \ Joules$) by continuing the current energy consumption trend, these resources will be almost depleted within a century. Although some kind of energy sources, as wind, hydro, geothermal and solar energy are unpollutant and free of charge, they will not be enough to satisfy the human energy needs in the next century, because of their low energy density, low profit over cost ratio and strong dependence on diurnal, seasonal, climatical and geological conditions.

CHAPTER 2

AN OVERVIEW TO FUSION PHYSICS

In this chapter, an overview of the fundamentals of fusion physics and the concepts which will be used in the next chapters will be given.

2.1 Fusion Reaction

Fusion energy is obtained by fusing the atomic nuclei of light elements, such as hydrogen and its isotopes deuterium and tritium. Figure 2.1 shows the mass defect, or the binding energy, versus atomic number [3].

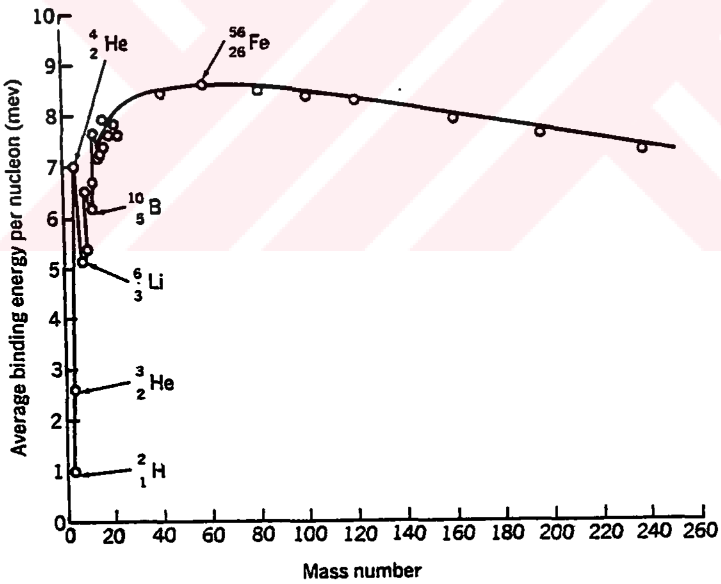

Figure 2.1 Binding energy versus atomic number.

As seen in the Figure 2.1, light nuclei when fused together and the heavy ones when fissioned lose some of their mass. This mass defect is converted to energy according to well-known Einstein's formula

$$E = mc^2 \tag{2.1}$$

Since the mass defect encountered in fusion is much greater than that results in fission, the release energy by fusion is much higher than produced by fission. Basic fusion reactions, which can take place in a reasonably sized terrestrial fusion reactor are as follows [4]:,

$$\begin{array}{llllll}
D+T & \longrightarrow & {}^4He & (3.52\ MeV) & + & n \quad (14.06\ MeV) \\
D+D & \longrightarrow & T & (1.01\ MeV) & + & p \quad (3.02\ MeV) \\
D+D & \longrightarrow & {}^3He & (0.82\ MeV) & + & n \quad (2.45\ MeV) \\
D+{}^3He & \longrightarrow & {}^4He & (3.67\ Mev) & + & p \quad (14.67\ MeV)
\end{array}$$

The obtained energy is per one atom and hence for $1 atom - gram$ it must be multiplied by the Avogadro Number (6.02×10^{23}). This is the source of the incomparable energy amount that fusion gives.

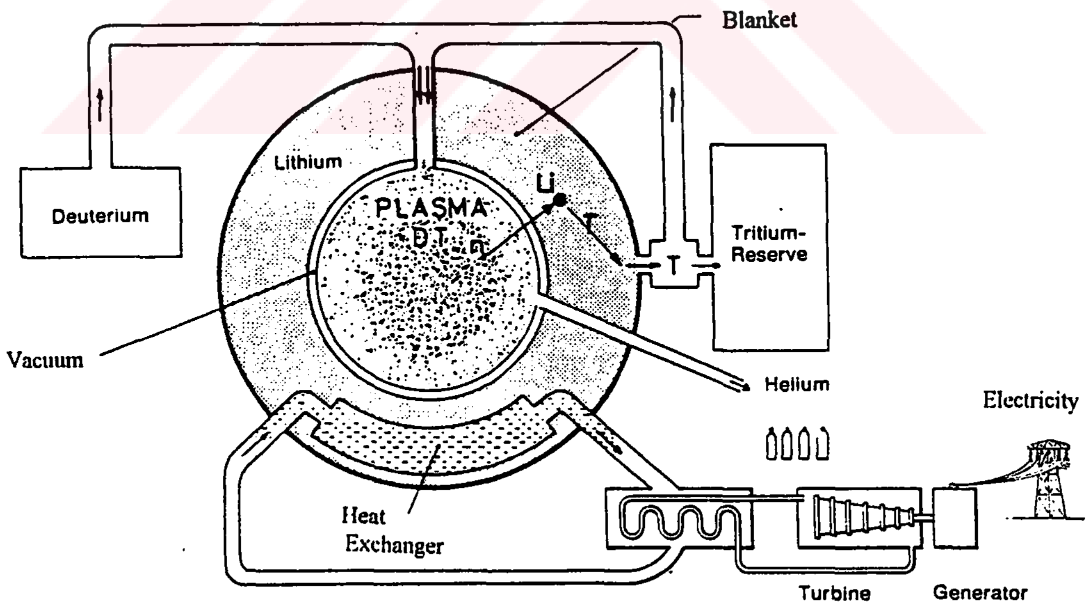

Figure 2.2 Schematic view of fusion reactor.

Since the fusion reaction rate parameter is the largest for the $D - T$

reaction, the first fusion reactor will burn $D-T$ fuel. To produce 1 $GW-year$ of electrical energy from fusion reaction requires only 1 *tonne* of deuterium. To get the same amount of energy in a coal–fired power plant needs 2×10^6 *tonnes* of carbon with the same order of amount of pollutant materials injecting into nature. Deuterium is the stable isotope of hydrogen and can be found in the seawater one per 6700 atoms of hydrogen. Although tritium is unstable and can not be found in nature, it can be bred in a fusion reactor, as shown in the Figure 2.2, from a lithium blanket surrounding the plasma by the bombardement of highly energetic neutrons [3].

Thus, the problem is to fuse two nuclei (protons) whose electric charges are the same. The Coulomb Law governs the relationship between charges. The same two charges repels each other according to following the formula,

$$\vec{F} = \frac{q^2}{4\pi\epsilon r^2}\hat{r} \tag{2.2}$$

where, ϵ : dielectric constant, q: electric charge, $\hat{r}$: the unit position vector. This formula states that the repelling force between two same charges is proportional to the inverse square of the distance between them. To fuse two protons, one must overcome this Coulomb force and must make two charges very close to each other enough to activate the other type of the forces which are dominant in that distances (Strong and weak forces). Only after then, the nuclei will fuse and give energy out. As a result, the plasma must be hot enough so that fusing collisions between nuclei are sufficiently probable (10^8 K, gives a probability of about 1%, which is sufficient) and well enough confined that the energy loss rate is less than the fusion power (The product of the plasma ion density n and the plasma energy confinement time τ_e must be at least 10^{20} sec/m^3). This criterion is known as Lawson Criterion. To fuse two nuclei, one needs extremely high temperatures. To increase the probability, it is necessary to aim one proton with sufficient energy to another.

At this temperature levels, all the elements known are nearly fully ionized state. It is impossible for any vessel made from any known material to contain a plasma having such high temperatures. There are two confinement method which widely used, one of which is inertial, the other is magnetic. Although there are a lot of studies about inertial confinement, in this study, one of the magnetic confinement methods was concerned.

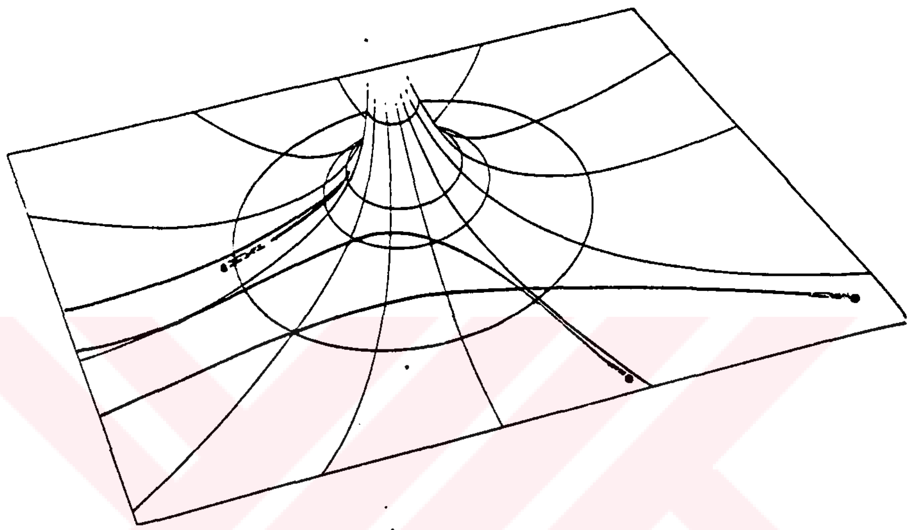

Figure 2.3 Insufficient energy or any error in aiming prevents fusion.

2.2 Tokamak

Tokamak is one of the toroidal plasma confinement devices. The main difference of it from the other toroidal magnetic confinement systems is to have a strong toroidal magnetic field produced by a large current in the plasma itself [5]. The radius of the torus is called major radius and the radius of the plasma column is called the minor radius. A transformer is used to induce the electric current into plasma. The iron yoke of the transformer is set perpendicular to the torus at the center of the major radius [6], as shown in Figure 2.3.

When the electric current flows on the primary coil, the magnetic flux in the iron yoke changes and a current is induced in the toroidal plasma column as the secondary coil. This induced current (toroidal one) generates the magnetic field $\vec{B}_\theta$ around the plasma column to pinch it. $\vec{B}_\theta$ is called the poloidal field

[6]. In addition to the usual toroidal field $\vec{B}_t$ and the plasma–produced poloidal field $\vec{B}_\theta$, a third field $\vec{B}_z$ in the vertical direction is needed to counteract the natural tendency for the current ring, the plasma, to expand. The field $\vec{B}_z$ is directed so that the $\vec{j} \times \vec{B}_z$ force is radially inward [5]. The confined plasma is generally stable because the poloidal magnetic field is a minimum at the minor axis in the toroidal plasma [6]. The rotational transform of a magnetic field line, ι, must not be an integral of 2π. Otherwise, the field lines would close upon themselves and would not cover the whole magnetic surface. In that case, electrons could not go wherever necessary to cancel space charge. The rate at which a line of force at the plasma surface winds around the major axis is proportional to B_t/R, and the rate at which it winds around the minor axis is proportional to B_θ/a. The rotational transform is therefore proportional to $B_\theta R/B_t a$. The safety factor indicates how far a tokamak is from the stability limit $q = 1$, which is called Kruskal–Shafranov limit [5].

$$q = \frac{B_t}{B_\theta}\frac{a}{R} = \frac{2\pi}{\iota} \tag{2.3}$$

A tokamak must be designed so that plasma which leaves the central part by diffusion, does not hit the first wall directly [6]. This is an experimental problem of considerable importance, since the influx of heavy elements from the walls causes rapid loss of energy by atomic radiation [5].

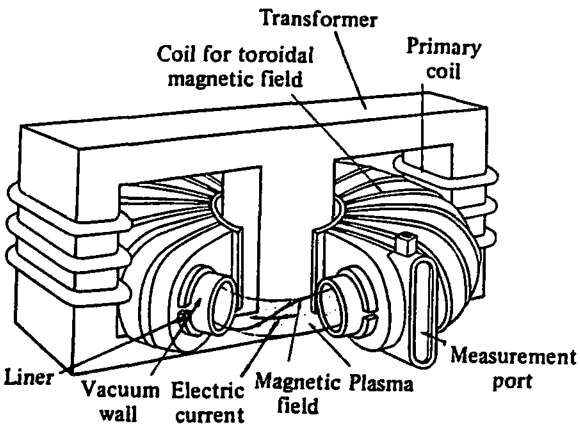

Figure 2.4 Principal scheme of tokamak

It has been seen, that, to keep the plasma clean, i.e., to prevent the plasma from the heavy particles torn from the wall of the vacuum vessel by the energetic particles, the fusion products, is important to reach the self–ignition of the fuel. To control the plasma contamination and to keep the plasma clean, divertors are widely used than limiters or gas clouds [6]. As shown in the Figure 2.5, a divertor pulls the outer part of the poloidal magnetic fields out of the plasma column by the action of a divertor coil forming two magnetic field regions separated by a surface called separatrix. The heavy particles, the impurities, from the wall follow the outer magnetic field lines and are deposited on the divertor plate. Therefore tokamak devices equipped with divertors have cleaner plasma and the energy given is spent for the particles which can fuse together at that temperatures.

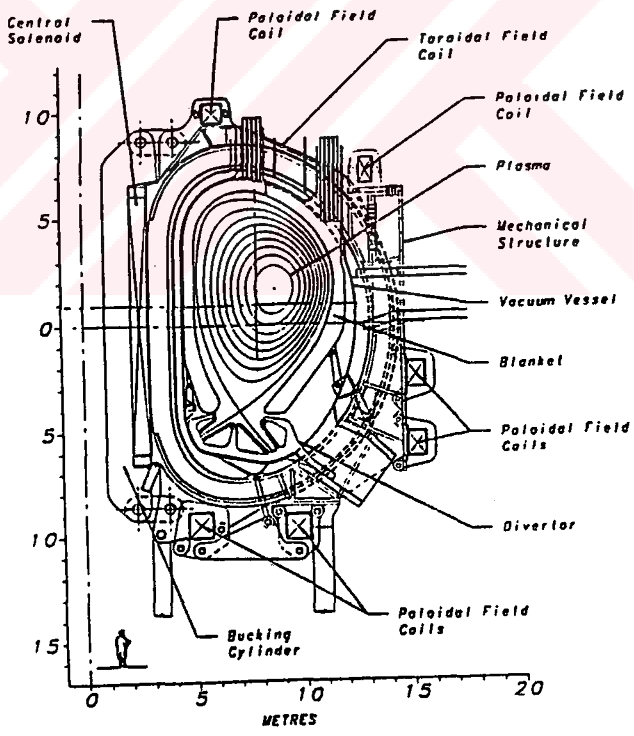

Figure 2.5 Cross section of a divertor tokamak device. (ITER EDA Design)

CHAPTER 3

MAGNETIC FIELDS AND THE MOTION OF CHARGED PARTICLES

3.1 Magnetic Field of A Current

The Maxwell's equations which relate the electromagnetic fields to the motion of charges are given as, [7],

$$\begin{aligned} \nabla \times \vec{E} + \frac{\partial \vec{B}}{\partial t} &= 0 \\ \nabla \times \vec{H} - \frac{\partial \vec{D}}{\partial t} &= \vec{j} \\ \nabla \cdot \vec{B} &= 0 \\ \nabla \cdot \vec{D} &= \rho \end{aligned} \tag{3.1}$$

where $\vec{E}$, $\vec{B}$, $\vec{D}$ and $\vec{H}$ are the electric intensity, the magnetic induction, the electric displacement and the magnetic intensity, respectively. ρ and $\vec{j}$ stand for the charge and the current densities. When the medium is uniform and isotropic

$$\vec{D} = \epsilon \vec{E} \quad ; \qquad \vec{B} = \mu \vec{H} \tag{3.2}$$

ϵ and μ are called dielectric constant and permeability, respectively [7].

If the fields do not change in time, the field equations reduce to

$$\begin{aligned}
\vec{E} &= -\nabla\phi \\
\vec{B} &= \nabla \times \vec{A} \\
\nabla^2\phi &= -\frac{1}{\epsilon} \\
\nabla^2\vec{A} &= -\mu\vec{j} \\
\nabla\cdot\vec{A} &= 0 \\
\nabla\cdot\vec{j} &= 0
\end{aligned} \tag{3.3}$$

where ϕ is scalar potential, $\vec{A}$ is vector potential [7]. The vector potential, $\vec{A}$, at an observation point P (given by the position vector $\vec{r}$) is expressed in terms of the current densities at the point Q (given by $\vec{r}'$), as shown in the Figure 3.1., by

$$\vec{A}(\vec{r}) = \frac{\mu}{4\pi}\int_V \frac{\vec{j}(\vec{r}')}{R}d\vec{r} \tag{3.4}$$

where $\vec{R} = \vec{r} - \vec{r}'$ and $R = |\vec{R}| = ((x-x')^2 + (y-y')^2 + (z-z')^2)^{1/2}$

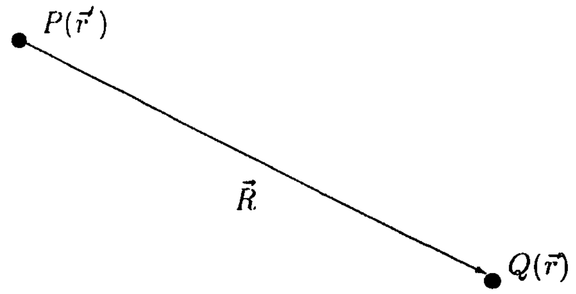

Figure 3.1 Observation point P and the location Q of a charge or current.

Since the field $\vec{B}$ is expressed as in Equation 3.3 we find, [7],

$$\vec{B} = \frac{\mu}{4\pi} \int_V \frac{\vec{j} \times \vec{R}}{R^3} dr' \tag{3.5}$$

If the current distribution is given by a current I flowing in closed loops, magnetic intensity is described by Biot–Savart equation,

$$\vec{H} = \frac{\vec{B}}{\mu} = \frac{I}{4\pi} \int_C \frac{\vec{s} \times \vec{n}}{R^2} ds \tag{3.6}$$

where $\vec{s}$ and $\vec{n}$ are the unit vectors in the directions of $\vec{j}$ and $\vec{R}$, respectively [7].

3.2 Magnetic Surfaces

Since the magnetic induction vector, $\vec{B}$, is tangent to the line of the magnetic force, it satisfies the following condition

$$d\vec{l} \times \vec{B} = 0 \tag{3.7}$$

and hence

$$\frac{dx}{B_x} = \frac{dy}{B_y} = \frac{dz}{B_z} = \frac{dl}{B} \tag{3.8}$$

where l denotes the length along the line of magnetic surface and B is the absolute magnitude of $\vec{B}$ [7]. The magnetic surface $\psi(\vec{r}) = constant$ is a surface upon which the magnetic force line lies and it should satisfy the following condition

$$(\nabla\psi(\vec{r})) \cdot \vec{B} = 0 \tag{3.9}$$

$\nabla\psi$ is normal to the magnetic surface [7]. If a magnetic field has some symmetry, the exact solution of the magnetic surface can easily be derived. In the case of axial symmetry, it is independent of the angle which is taken about the axis of symmetry. In this case

$$rA_\theta(r,z) = constant \tag{3.10}$$

Vector potential for a ring current through which a current I flows, as shown in Figure 3.2 is given as

$$A_\theta = \frac{\mu}{\pi k} I \left(\frac{a}{r}\right)^{1/2} \left(\left(1 - \frac{1}{2}k^2\right) K(k) - E(k)\right) \tag{3.11}$$

where,

$$k^2 = \frac{4ar}{(a+r)^2 + z^2} \tag{3.12}$$

where K and E are complete elliptic integrals of the first and second kind respectively [7].

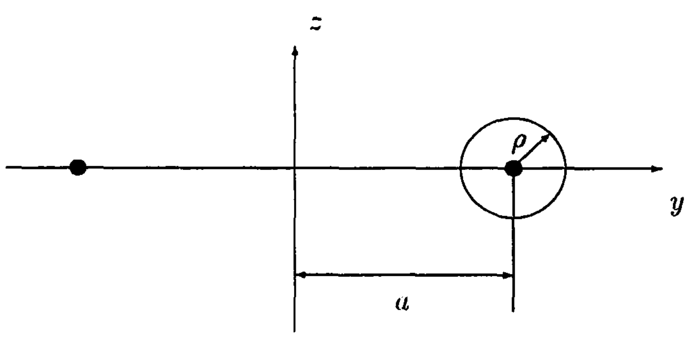

Figure 3.2 Ring current geometry.

The magnetic field components are given by, [7]

$$B_r = -\frac{\partial A_\theta}{\partial z} \;\; ; \quad B_\theta = 0 \;\; ; \quad B_z = \frac{1}{r}\frac{\partial}{\partial r}(rA_\theta) \tag{3.13}$$

with,

$$\frac{\partial K}{\partial k} = \frac{1}{k}\left(\frac{E}{1-k^2} - K\right) \; ; \quad \frac{\partial E}{\partial k} = \frac{1}{k}(E-K) \tag{3.14}$$

3.3 Equation of Motion of A Charged Particle

The equation of motion of a particle of mass m and charge q in an magnetic field $\vec{B}$ is, [7]

$$m\frac{d\vec{v}}{dt} = q(\vec{v} \times \vec{B}) \tag{3.15}$$

The Lagrangian formulation for generalized coordinates q_i is, [7]

$$\frac{d}{dt}\frac{\partial L}{\partial \dot{q}_i} - \frac{\partial L}{\partial q_i} = 0 \tag{3.16}$$

where L is given by

$$L = \frac{mv^2}{2} + q\vec{v} \cdot \vec{A} \tag{3.17}$$

The equations of motion in the Hamiltonian form use the generalized momentum, defined by

$$p_i = \frac{\partial L}{\partial \dot{q}_i} \tag{3.18}$$

as the independent variables, the Hamiltonian equations are

$$\begin{aligned} \frac{dp_i}{dt} &= -\frac{\partial \mathcal{H}}{\partial q_i} \\ \frac{dq_i}{dt} &= -\frac{\partial \mathcal{H}}{\partial p_i} \end{aligned} \tag{3.19}$$

here the Hamiltonian $\mathcal{H}$ is given by

$$\mathcal{H} = \frac{1}{2m}(\vec{p} - q\vec{A})^2 \tag{3.20}$$

where $\vec{p}$ is the momentum vector.

If there is also an electric field $\vec{E} = -\nabla\phi$, Hamiltonian takes the form following, [7]

$$\mathcal{H} = \frac{1}{2m}(\vec{p} - q\vec{A})^2 + q\phi \tag{3.21}$$

In the axisymmetric system,

$$p_\theta = \frac{\partial L}{\partial \dot{\theta}} = mr^2\dot{\theta} + qrA_\theta = constant \tag{3.22}$$

If the Hamiltonian does not dependent explicitly on time t, then $\mathcal{H} = constant$ is one integral of the Hamiltonian equation. This integral expresses the conservation of energy which may be written as

$$\frac{mv^2}{2} = w \tag{3.23}$$

3.4 Cyclotron Motion

Equation 3.1 states that the force exerted to a particle in the magnetic field is perpendicular to its velocity. This implies that the particle will experience a curved orbit [6]. If the field is constant in space and time, the path will be circle in the plane perpendicular to the magnetic field direction. This motion is known as cyclotron motion and its frequency is called cyclotron frequency whose magnitude is

$$\omega_c = \frac{|q|B}{m} \tag{3.24}$$

The radius, known as Larmor Radius, of circular motion is given as

$$r_L = \frac{mv_\perp}{|q|B} \tag{3.25}$$

The center of this circle is called guiding center. Here, $v_\perp$ stands for the perpendicular component of velocity to the magnetic field line around which the particle rounds. Since the velocity along $\vec{B}$ is not affected by field, the general path is a helix. The direction of the gyration is always such that the magnetic field generated by the charged particle is opposite to the externally imposed field as seen in the Figure 3.3.

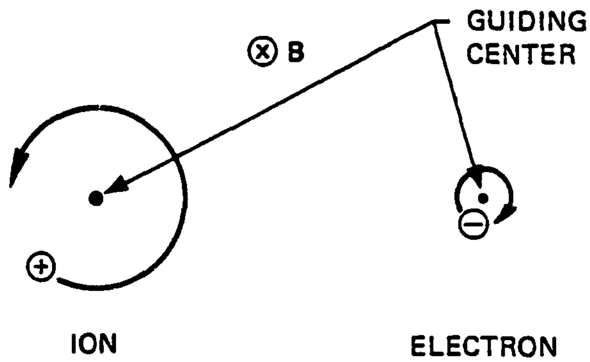

Figure 3.3 Guiding center in cyclotron motion.

3.5 Drift Motion Due To Curvature

In the case in which the magnetic field has a curvature of radius, R_c, a charged particle moving along the magnetic field with velocity $v_\parallel$ is affected by a centrifugal force

$$\vec{F} = \frac{mv_\parallel^2}{R_c}\hat{r} = \frac{mv_\parallel^2}{R_c^2}\vec{R}_c \tag{3.26}$$

This force gives rise to a drift

$$\vec{v}_c = \frac{mv_\parallel^2}{qB^2}\frac{\vec{R}_c \times \vec{B}}{R_c^2} \tag{3.27}$$

3.6 Grad B Drift

The difference in magnetic field intensity will cause the Larmor radius to change. The radius is small at a point where the magnetic field is strong, and large where the field is weak [6]. Thus the particle undergoes a drift motion perpendicular to $\vec{B}$ and ∇B as shown in Figure 3.4.

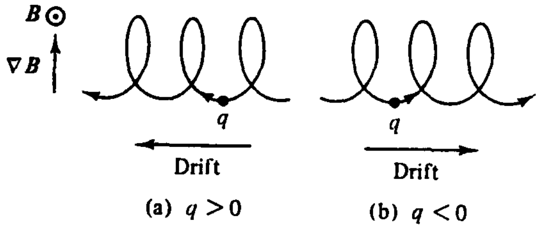

Figure 3.4 Grad B drift

The drift velocity of guiding center is given as follows

$$\vec{v} = \frac{v_\perp r_L}{2}\frac{\vec{B} \times \nabla B}{B^2} \tag{3.28}$$

3.7 Equation and Constants of Motion

The motion of charged particle in a magnetic field, under the influence of an external force, can be described as the superposition of a gyration around the guiding center with the cyclotron frequency and the motion of the guiding center.

The resulting equation of motion of a charged particle may be reached by using Hamiltonian approach [8], as follows

$$\frac{d\vec{x}}{dt} = v_{\parallel}\vec{b} + \frac{\vec{b}}{eB} \times \left[mv_{\parallel}^{2}\vec{b}\cdot\nabla\vec{b} + \mu_m \nabla B\right] \tag{3.29}$$

where $\mu_m = mv_{\parallel}^2/(2B)$ the magnetic moment, $\vec{b}$ the unit vector along the magnetic field vector. $v_{\parallel}$ and $v_{\perp}$ stand for the components of the particle velocity, which are the parallel and the perpendicular to the magnetic field line, respectively. The particle energy, in this case, can be written as

$$\varepsilon = \frac{1}{2}mv_{\parallel}^{2} + \mu_m B \tag{3.30}$$

Since the magnetic force acting the particle is perpendicular to the velocity, no work is done by the magnetic field. The first constant of motion of a charged particle in an arbitrary magnetic field is the particle energy given in the Equation 3.30. By multiplying both sides of the Equation 3.15 by the particle velocity $\vec{v}$

$$m\vec{v}\frac{d\vec{v}}{dt} = q\vec{v}\cdot(\vec{v}\times\vec{B})$$

$$m\vec{v}\frac{d\vec{v}}{dt} = \frac{d}{dt}\left(\frac{1}{2}mv^{2}\right) = 0$$

$$\varepsilon = constant \tag{3.31}$$

In the case of Larmor gyration, since there is a periodicity in time, the action integral in terms of the canonical variables p, q is

$$J = \oint p\, dq \tag{3.32}$$

J is the adiabatic invariant. If we take p to be the angular momentum $mv_{\perp}r_L$ and dq to be the coordinate $d\theta$, this integral becomes

$$\oint p\, dq = \oint mv_{\perp}r_L d\theta = 2\pi r_L mv_{\perp} = 2\pi \frac{mv_{\perp}^2}{\omega_c} = 4\pi \frac{m}{|q|}\mu_m$$

Since the ratio $m/|q|$ is constant in nonrelativistic cases as the one we interested, the magnetic moment μ_m will be constant along its path. Thus, the second invariant of motion is the magnetic moment [5].

There is one more periodic motion in the axially symmetric cases. The adiabatic invariant connected with this turns out to be the total magnetic flux enclosed by the drift surface. As $\vec{B}$ varies, the particle will stay on a surface such that the total number of lines of force enclosed remains constant. In the nonaxisymmetric cases, however, this constancy will be violated [5].

3.8 Banana Orbits

Figure 3.5 shows a torus with a helical line of force. The twist is needed to eliminate the unidirectional grad$-B$ and curvature drifts. As a particle moves along a line of force, it sees a larger $|B|$ near the onside wall of the torus and smaller $|B|$ near the outside wall [5]. Because a charged particle moves almost along the magnetic field line, the particle moves toward the direction along which the magnetic field intensity increases; so the particle executes a spiral motion from outside to inside the torus. The particle is subject to decelerating force when it moves along a magnetic field line whose intensity is increasing. Hence charged particles with small initial velocities cannot pass the point of maximum intensity of the magnetic field, and so bounce on the way. This trajectory looks like a banana in the constant toroidal angle plane, and it is called as 'Banana Orbit' [6].

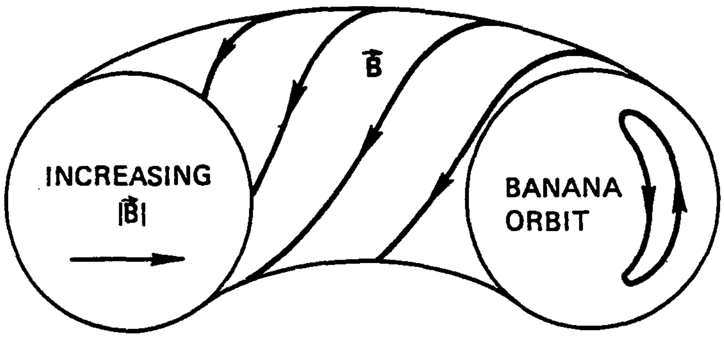

Figure 3.5 A banana orbit of a particle confined in a toroidal device.

CHAPTER 4

AN OVERVIEW TO BASIC CONCEPTS OF NONLINEAR DYNAMICS

In this chapter, the basic concepts of dynamical systems which will be used in the next chapters will be given.

4.1 Preliminary Definitions

A dynamical system may usually be described by the following equation [9]

$$\frac{dx}{dt} = \dot{x} = f(x, t, \mu) \tag{4.1}$$

$x \in U \subset \mathcal{R}^n$, $t \in \mathcal{R}^1$, and $\mu \in V \in \mathcal{R}^p$ where U and V are open sets in $\mathcal{R}^n$ and $\mathcal{R}^1$, respectively. μ is parameter. In dynamical systems, the independent variable t is usually referred as time. Equation 4.1 may be also called vector field. Vector fields which do not depend explicitly on time are called autonomous and those which are dependent of time are called nonautonomous [9].

The space of dependent variables of 4.1, $\mathcal{R}^n$, is called phase space of dynamical system and to find the geometry of solution curves in phase space is the main goal. $x(t, t_0, x_0)$, the solution of 4.1 may sometimes be referred to as trajectory of phase curve through the point x_0 at $t = t_0$ [9].

The graph of $x(t, t_0, x_0)$ over t is referred to as an integral curve, or, the graph $x(t, t_0, x_0) = \{(x, t) \in \mathcal{R}^n \times \mathcal{R}^1 \mid x = x(t, t_0, x_0), t \in I\}$ where I is the time interval of existence [9].

The orbit through x_0, x_0 is a point in the phase space of 4.1, is the set of points in phase space that lie on a trajectory passing through x_0, symbolically,

$x_0 \in U \subset \mathcal{R}^n$, the orbit through x_0 is given by
$\mathcal{O}(x_0) = \{x \in \mathcal{R}^n \mid x = x(t, t_0, x_0), t \in I\}$ [9].

Let's consider the equation

$$\dot{x} = \begin{bmatrix} 0 & 1 \\ -1 & 0 \end{bmatrix} x \quad \text{where} \quad x = [u \quad v]^T \; ; \quad x \in \mathcal{R}^2$$

the solution passing through the point x_0 at $t = 0$ is given by
$x = [\cos t \, , \quad -sint]^T$ [9].

The integral curve passing through $x = [1 \quad 0]^T$ at $t = 0$ is given by $\{(x,t) \in \mathcal{R}^2 \times \mathcal{R}^1 \mid x = [\cos t \quad -\sin t]^T, \; t \in \mathcal{R}\}$. The orbit passing through $x = [1 \quad 0]$ is given by the circle $x \cdot x = 1$ [9].

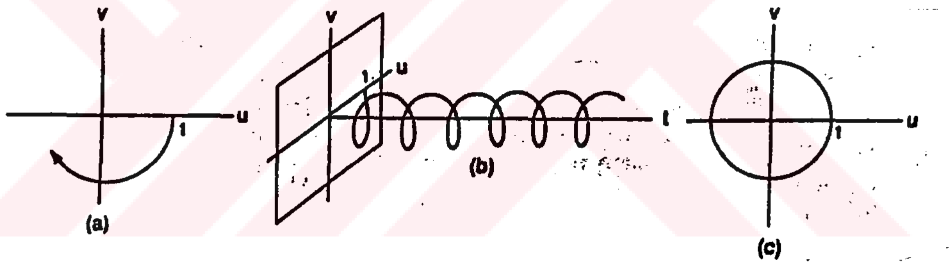

Figure 4.1 Geometrical interpretation of a) Solution; b) Integral Curve; c) Orbit [9]

In the geometrical point of view, with a given specific dynamical system, understanding the complete characterization of the geometry of orbit structure is the main subject of the study, as well as finding the change in the orbit when the parameters are varied is the main goal.

Let's consider a general autonomous vector field

$$\dot{x} = f(x) \; ; \quad x \in \mathcal{R}^n \tag{4.2}$$

An equilibrium solution of 4.2 is a point $\bar{x} \in \mathcal{R}^n$ such that $f(\bar{x}) = 0$, i.e., a solution which does not change in time. Other terms often substituted for the term "equilibrium solution", are "fixed point", "stationary point", "rest point", "singularity", "critical point" or "steady state". Let's say that we find any fixed point of 4.2. The next step is to determine if this solution is stable or not. Two kind of stability may be described,

1. Liapunov Stability: $\bar{x}(t)$ is said to be stable (or Liapunov stable) if $\forall\varepsilon > 0, \quad \exists\delta(\varepsilon) > 0$, for any other solution $y(t)$, of 4.2 satisfying

$$|\bar{x}(t_0) - y(t_0)| < \delta, \quad |\bar{x}(t) - y(t)| < \varepsilon$$

   for $t > t_0, \quad t_0 \in \mathcal{R}^1$

2. Asymptotic Stability: $\bar{x}(t)$ is said to be asymptotically stable if $\exists b > 0$ such that

$$|\bar{x}(t_0) - y(t_0)| < \delta\ , \quad \lim_{t\to\infty} |\bar{x}(t) - y(t)| = 0$$

Or, we can express the above two definitions as: $\bar{x}(t)$ is Liapunov stable, if solution starting "close" to $\bar{x}(t)$ at a given time remain "close" to $\bar{x}(t)$ for all times; and it is asymptotically stable if nearby solutions converge to $\bar{x}(t)$ as $t \to \infty$. A critical point of 4.2 which is not stable is called unstable [9].

In order to determine the stability of $\bar{x}(t)$, we must understand the nature of solutions near $\bar{x}(t)$. Let's start to study by shifting the origin of the coordinate axis to $\bar{x}(t)$ letting,

$$x = \bar{x}(t) + y \tag{4.3}$$

Substituting 4.3 into 4.2 and expanding it about $\bar{x}(t)$ gives

$$\dot{x} = \dot{\bar{x}}(t) + \dot{y} = f(\bar{x}(t)) + Df(\bar{x}(t))y + \mathcal{O}(|y|^2) \tag{4.4}$$

where Df is the derivative of f and $|\ \ |$ a norm on $\mathcal{R}^n$. (Supposing f is C^r) Recalling $\dot{\bar{x}}(t) = f(\bar{x}(t))$, 4.4 becomes

$$\dot{y} = Df(\bar{x}(t))y + \mathcal{O}(|y|^2) \tag{4.5}$$

The behaviour of solution close to $\bar{x}(t)$ may be found by studying the associated linear system

$$\dot{y} = Df(\bar{x}(t)) \tag{4.6}$$

A physical system modelled mathematically by a differential operator, D, in the space of m–continuously differentiable functions, C^m, is said to be linear, if the following relationship holds.

$$D(ax + by) = aD(x) + bD(y) \tag{4.7}$$

where a, b are constants and $x, y \in \mathcal{R}^n$

Therefore, we will find if solution of 4.6 is stable or not and then show that this solution exactly on the same way as 4.2. With the definition of the equilibrium solution, $\bar{x}(t) = \bar{x}$ and $Df(\bar{x}(t)) = Df(\bar{x})$, means that the derivative matrix contains only constants. Hence, the solution of 4.6 through $y_0 \in \mathcal{R}^n$ of $t = 0$ can be written as

$$y(t) = e^{Df(\bar{x})t}y_0 \tag{4.8}$$

If all eigenvalues of $Df(\bar{x})$ have negative real parts, the $y(t)$ is asymptotically stable. If all of the eigenvalues of $Df(\bar{x})$ have negative real parts, the equilibrium solution $x = \bar{x}$ of 4.2 is asymptotically stable [9].

If the eigenvalues of the associated linear vector field have nonzero real parts, then the orbit structure near an equilibrium solution of the nonlinear vector field is essentially the same as that of the linear vector field. A hyperbolic fixed point is the point $\bar{x}$, a fixed point of $\dot{x} = f(x)$, $x \in \mathcal{R}^n$, if none of the eigenvalues of $Df(\bar{x})$ have zero real part. A hyperbolic fixed point of a vector field is called saddle if some, but not all, of the eigenvalues of the associated linearization have real parts greater than zero and the rest of the eigenvalues have real parts less than zero. If all of the eigenvalues have negative real part then the hyperbolic fixed point is called a stable node or sink, and if all of the eigenvalues have positive real parts then the hyperbolic fixed point is called an unstable node or source. If the eigenvalues are purely imaginary and nonzero the nonhyperbolic fixed point is called a center [9].

4.2 Types of The Fixed Points in 2D Phase Space

Let's start by considering the autonomous system of the form

$$\begin{aligned}\frac{dx}{dt} &= P(x,y)\\ \frac{dy}{dt} &= Q(x,y)\end{aligned}\tag{4.9}$$

and the critical point (x_0, y_0) of this system. From the definiton of the critical point, we know that $P(x_0, y_0) = 0$ and $Q(x_0, y_0)$. The first assumption will be that this critical point (x_0, y_0) is isolated, i.e., (x_0, y_0) is the only critical point in the circle whose center is (x_0, y_0) and whose radius is sufficiently small and the functions P and Q are continuous and have partial derivatives in this circle [10]. For convenience, let's take $x_0 = 0$, and $y_0 = 0$. There is no loss in generality, because the translation of coordinates $\xi = x - x_0$; $\eta = y - y_0$ transforms (x_0, y_0) into the origin in the $\xi\eta$ plane [11]. Hence the system 4.8 can be written in the form

$$\begin{aligned}\frac{dx}{dt} &= ax + by + P_1(x,y)\\ \frac{dy}{dt} &= cx + dy + Q_1(x,y)\end{aligned}\tag{4.10}$$

where

$$
\begin{aligned}
a &= \left[\frac{\partial P}{\partial x}\right]_{(0,0)} \quad ; \quad b = \left[\frac{\partial P}{\partial y}\right]_{(0,0)} \\
c &= \left[\frac{\partial Q}{\partial x}\right]_{(0,0)} \quad ; \quad d = \left[\frac{\partial Q}{\partial y}\right]_{(0,0)}
\end{aligned}
\tag{4.11}
$$

The following requirement about the Jacobian, J, is needed for the critical point to be isolated

$$
J = \left.\frac{\partial(P,Q)}{\partial(x,y)}\right|_{(0,0)} = 0 \tag{4.12}
$$

Hence the system 4.8 has been linearized in the neighborhood of (x_0, y_0), as follows

$$
\begin{aligned}
\frac{dx}{dt} &= ax + by \\
\frac{dy}{dt} &= cx + dy
\end{aligned}
\tag{4.13}
$$

This system has the following characteristic equation

$$
\lambda^2 - (a + d)\lambda + (ad - bc) = 0 \tag{4.14}
$$

The stability of the linearized system depends on the roots of the characteristic equation is shown in the Table 4.1 [11].

Table 4.1 Stability Types Depending on The Roots of Characteristic Equation for 2D Phase Space.

Nature of The Roots of Characteristic Equation	Nature of Critical Point of Linear System	Stability of Critical Point
Real, Unequal and of Same Sign	Node	Asymptotically Stable If Roots Are Negative Unstable If Positive
Real, Unequal and of Opposite Sign	Saddle Point	Unstable
Real and Equal	Node	Asymptotically Stable If Roots Are Negative Unstable If Positive
Conjugate Complex But Not Pure Imaginary	Spiral Point	Asymptotically Stable If Real Part of Roots Is Negative Unstable If Positive
Pure Imaginary	Center	Stable, But Not Asymptotically Stable

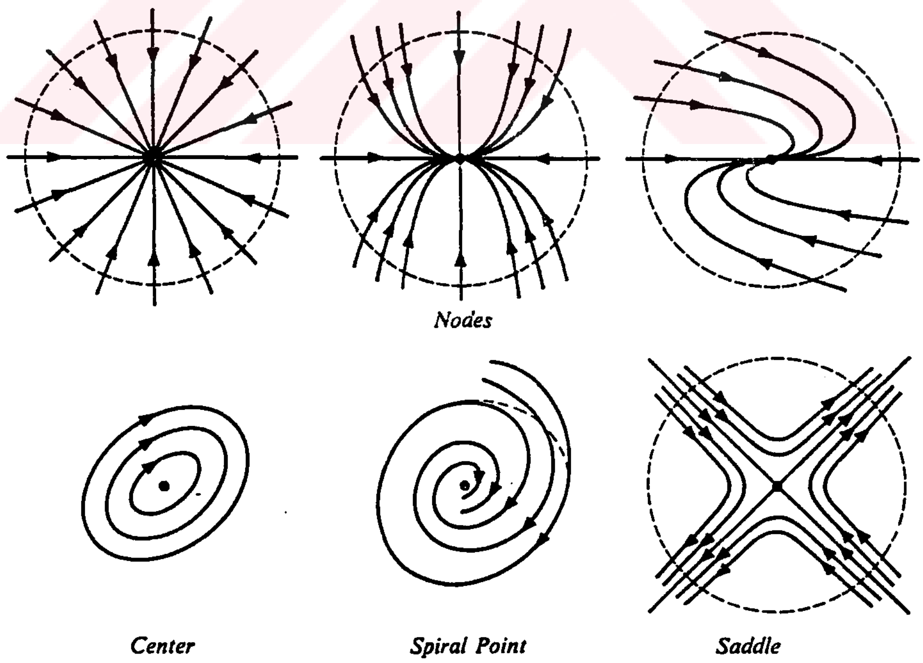

Figure 4.2 Views of Critical Points in 2D Phase Space.

What one can say about the main nonlinear system is the following [11]:

1. The critical point $(0,0)$ of the nonlinear system 4.8 is of the same type as that of the linear system 4.9 in the following cases:
   If the roots of characteristic equation

   (i) are real, unequal and of the same sign. critical points of both linear and nonlinear system are node.

   (ii) are real, unequal and of opposite sign. critical points of both linear and nonlinear system are saddle points.

   (iii) are real and equal and the linear system is not such that $a = d \neq 0$, $b = c = 0$, then both critical points of two system are nodes.

   (iv) are conjugate complex with real part not zero, then both critical points are spiral points.

2. The critical point $(0,0)$ of the nonlinear system 4.8 is not necessarily of the same type as that of the linear system 4.9 in the following cases:
   If the roots of characteristic equation

   (vi) are real and equal and linear system is such that $a = d \neq 0$, $b = c = 0$, then although $(0,0)$ is a node of linear system, it may be either a node or a spiral point of nonlinear system.

   (vii) are pure imaginary, then although $(0,0)$is a center of linear system, it may be either a center or a spiral point of nonlinear system.

Although the critical point of the nonlinear system is of the same type as that of the linear system in cases (i), (ii), (iii), and (iv), the actual appearence of the critical point in larger scale may be different. Following conclusions are based on the theorem of Liapunov discussing the stability of the critical point of nonlinear system [11]:

1. If both roots of the characteristic equation of the linear system are real and negative or conjugate complex with negative real parts, then the point $(0,0)$ is asymptotically stable for both linear and nonlinear systems.

2. If the roots of the characteristic equation are pure imaginary, then although $(0,0)$ is a stable critical point of linear system, it is not necessarily a stable critical point of the nonlinear system. The critical point of nonlinear system, in this case, may be asymptotically stable, stable but not asymptotically stable, or unstable.

3. If either of the roots of the characteristic equation is real and positive or if the roots are conjugate complex with positive real parts, then the critical points of both system are unstable.

4.3 Local Bifurcations

Describing verbally, bifurcation of a dynamical system is to be a change in the topology of the phase space when changing the parameters of the dynamical system [12]. The point (x,μ), the value of the parameter μ, on which this change is occured is called bifurcation point and bifurcation value, respectively [9]. The graph in which the parameter plotted versus the dependent variable is referred as bifurcation diagram.

By the term "Local", here, it is meant the bifurcations occuring in a neighborhood of a fixed point. Let's start by considering the parameterized vector field

$$\dot{y} = g(y,\lambda): \quad y \in \mathcal{R}^n \; ; \quad \lambda \in \mathcal{R}^p \tag{4.15}$$

g is a C^r function on some open set in $\mathcal{R}^n \times \mathcal{R}^p$. The degree of differentiability, r, is 5, which is sufficient for many cases.

Suppose 4.8 has a fixed point at $(y,\lambda) = (y_0,\lambda_0)$

$$g(y_0,\lambda_0) = 0 \tag{4.16}$$

Two question may be asked:

1) Is this fixed point stable or unstable?

2) How is the stability or instability affected as λ is varied?

Linearizing 4.8 about the fixed point will answer the first question. The linear vector field is given by

$$\dot{\xi} = D_y g(y_0, \lambda_0)\xi\ , \quad \xi \in \mathcal{R}^n \tag{4.17}$$

If the fixed point is hyperbolic (i.e., none of the eigenvalues of $D_y g(y_0, \lambda_0)$ lie on the imaginary axis), we know that stability of (y_0, λ_0) in 4.8 is determined by the linear equation 4.10. Since hyperbolic fixed points are structurally stable, varying λ slightly does not change the nature of the stability of the fixed point, thus the second answer is obvious [9].

The simplest case is to start with $D_y g(y_0, \lambda_0)$ has a single zero eigenvalue with the remaining eigenvalues having nonzero real parts. Several type of local bifurcations of fixed points are following,

a) Saddle–node bifurcation: In this kind of bifurcation, before and after a bifurcation value, the numbers and the types of the fixed points change. A simple example of saddle–node bifurcation can be seen in the following example. Let's consider the following example

$$\dot{x} = f(x, \mu) = \mu - x^2\ ; \quad x \in \mathcal{R}^1\ , \quad \mu \in \mathcal{R}^1 \tag{4.18}$$

here $f(0,0) = 0$ and $\frac{\partial f}{\partial x}(0,0) = 0$. The set of all fixed points is given by

$$\mu = x^2 \tag{4.19}$$

As seen in the graph of 4.17, (the bifurcation diagram of 4.16) Figure 4.1, there is no fixed points for $\mu < 0$ and two for $\mu > 0$ one of which is stable and the other is not. Here the bifurcation point is $(x, \mu) = (0,0)$ and the bifurcation parameter is $\mu = 0$.[9]

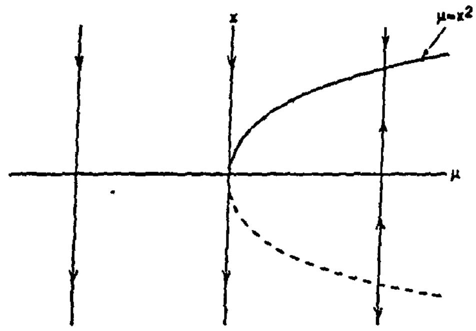

Figure 4.3 Diagram of saddle–node bifurcation.

b) **Transcritical bifurcation:** The bifurcation on which the type of the stability of fixed points exchanges is called as transcritical bifurcation. The vector field

$$\dot{x} = f(x, \mu) = \mu x - x^2 ; \quad x \in \mathcal{R}^1 , \quad \mu \in \mathcal{R}^1 \tag{4.20}$$

here $f(0,0) = 0$ and $\frac{\partial f}{\partial x}(0,0) = 0$. Fixed points are given by

$$x = 0 ; \quad x = \mu \tag{4.21}$$

As shown in Figure 4.2, for $\mu < 0$ there are two fixed points; $x = 0$ is stable and $x = \mu$ is unstable and for $\mu > 0$, $x = 0$ is unstable and $x = \mu$ is stable [9].

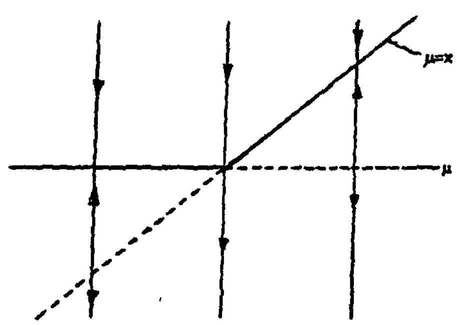

Figure 4.4 Diagram of transcritical bifurcation.

c) Pitchfork bifurcation: In this kind of bifurcation, when the parameters of the vector field passing through a certain value both the numbers of fixed points change and the stability of the existing fixed points exchanges. The associated example is

$$\dot{x} = f(x, \mu) = \mu x - x^3 ; \quad x \in \mathcal{R}^1 , \quad \mu \in \mathcal{R}^1 \tag{4.22}$$

here, as before, $f(0,0) = 0$ and $\frac{\partial f}{\partial x}(0,0) = 0$. The fixed points are given by

$$x = 0 , \quad x^2 = \mu \tag{4.23}$$

as seen in Figure 4.3m for $\mu < 0$, there is one stable fixed point, $x = 0$ and for $\mu > 0$, $x = 0$ remaining a fixed point, exchanges its stability and two new fixed points both of which are stable have been created. They are given by $x^2 = \mu$ [9].

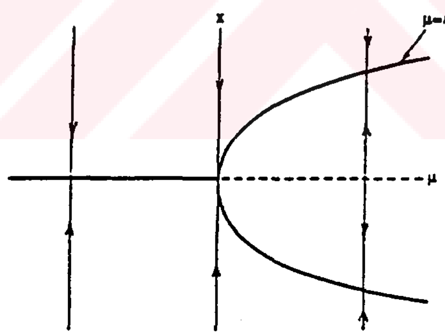

Figure 4.5 Diagram of Pitchfork bifurcation.

d) The following example for that nonhyperbolicity is required but not sufficient condition for bifurcation.

$$\dot{x} = f(x, \mu) = \mu - x^3 ; \quad x \in \mathcal{R}^1 , \quad \mu \in \mathcal{R}^1 \tag{4.24}$$

$f(0,0)$ and $\frac{\partial f}{\partial x}(0,0) = 0$ still holds and all the fixed points are given by

$$3 \tag{4.25}$$

as shown in Figure 4.4, there is no change in both the numbers and the stability of fixed points [9].

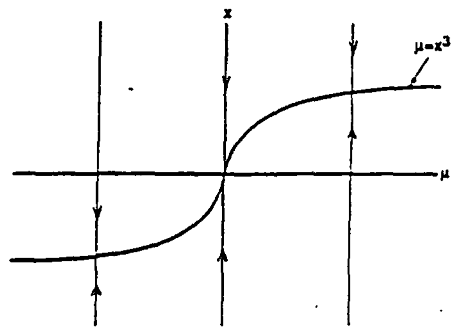

Figure 4.6 Diagram of nonhyperbolic case (No bifurcation).

4.4 Global Bifurcations

The topological character of the phase portrait of a system can change when a control parameter is varied, so that a bifurcation occurs, without changing the type of any of the fixed points of the system. In this case the change in the phase portrait is not noticeable in the neighborhood of any fixed point, but can only be discerned on global scale. Such global bifurcations are more difficult to detect and do not fall within any generalization which considers only the local degeneracy of fixed points [12].

4.5 Poincaré Section

A Poincaré map can be defined as the collection of the points representing the intersection of the selected Poincaré surface and the trajectories in the phase space. This mapping is also useful for seeing the behaviour of trajectories in a phase space of dimensionality greater than 4 by eliminating at least one of the variables of the problem resulting in the study of a lower dimensional problem [9]. Consider a vector field near some nontrivial orbit (not a fixed point) and the surface which is not tangent to the local vector field. The dimension of this surface is one less than that of the original phase space.

Generally, there may be a closed manifold of $\mathcal{R}^n$, denoted by S^*, such that all points intersect S^* in the same directional sense within some fixed, sufficiently large, interval of time, even if there is no periodic motion. This implies that "all" points intersect S^* an infinite number of times. The map $P : S^* \rightarrow S^*$ is Poincaré map, and this manifold, S^* is called Poincaré surface of section [12]. Consider a plane cutting the trajectories in 2D phase space of a dynamical system. Every time the trajectory passes through this plane, mark the trajectory's coordinate (p_n, q_n) on the plane. Then the two latest intersections can be related as follows:

$$(p_{n+1}, q_{n+1}) = T_n(p_n, q_n) \tag{4.26}$$

The operator T_n is determined by the equations of motion and defines the Poincaré mapping. The Poincaré mapping acts in a space of a smaller dimensionality than that of phase space. This simplification is paid for by the effort necessary to find the form of the operator T [13].

4.6 Chaos

Chaos is defined as an extremely dependent situation on the initial conditions. The assertion, that a dynamical system's behaviour is chaotic, means that the behaviour of the system is unpredictable however accurate its initial conditions are known. This theory tries to understand and to explain the systems that are deterministic, obeying the fundamental physical laws but with a predisposition for disorder, complexity and unpredictability. This is due to that minute changes amplify rapidly through feedback as the system evolves in time. This means that systems starting off with only slightly differing conditions rapidly diverge in character at a later stage. Such behaviour imposes strict limitations on predicting a future state, since the prediction depends on how accurately one can measure the inital conditions.

A linear system does not cause chaos due to the following reasons:

i) Chaotic behaviour arises from the nonlinear nature of the physical systems, however this does not imply that all the nonlinear systems have chaotic behaviour. For example, if one applies a periodic force to a linear, say a mass–spring, system, it will have a steady vibration with the same frequency as the applied force, after transients. This final motion does not depend on the system's initial conditions when the force was first applied. If nonlinearities are included to the system, then more than one steady–state solution is produced, and the one on which the system settles will depend on its initial conditions. Such a solution need not have the same periodic time as the applied force, although it will usually be some multiple of it. When the transients decay, the system may not settle into any regular oscillation but may continue to vibrate erratically, never quite repeating any earlier maneuvre. This is a chaotic solution.

ii) A linear dynamical system may have, if it has, only one fixed point in its phase space. And, the stability of the whole phase space is determined by this fixed point's stability. A nonlinear dynamical system, whereas, has at least two fixed points. And stability of a trajectory is affected by these fixed points simultaneously.

CHAPTER 5

FORMULATION AND RESULTS

In this study, charged particle motions in a divertor tokamak was investigated numerically. Three approach submitted in the following sub–chapters was used. In the first two, the drift motions are neglected, i.e., it is assumed that particle motions are predominantly parallel to the magnetic field lines [14]. At the last, the exact particle motion with drifts investigated. In all of three approaches, the calculations were performed numerically. Adams–Moulton numerical integration technique was used for integration.

The main goal of this study is to see the effects of nonaxisymmetric perturbation on divertor tokamaks. The plasma in a modern tokamak is bounded by a separatrix between magnetic field lines that form toroidal magnetic surfaces. An ideal tokamak is axisymmetric and the separatrix in an ideal tokamak is a sharp surface. Asymmetries in the magnetic field – which is created by the deviations in the tokamak coils from axisymmery, magnetic perturbations due to plasma instabilities and the effects of special coils introduced to control the width of the stochastic region– cause the last confining magnetic surface to lie inside the ideal separatrix to create a stochastic layer about the unperturbed separatrix. Magnetic field lines in this layer wander throughout a volume, rather than lying on a surface [14], [15]. All of three models consist $n = 1$ field error perturbation whose magnitude is typical of field errors that exist in present–day tokamaks [14].

5.1 First Approach

A simple model of a tokamak defined by three infinitely long, straight wires with codirectional currents. Here, the plasma body is represented by the middle wire carrying the current I_p. The divertors are simulated by two other wires situated at $\mp z_c$, each carrying the current I_c with $\gamma \equiv I_c/I_p = 0.67$, as shown in the Figure 5.1.

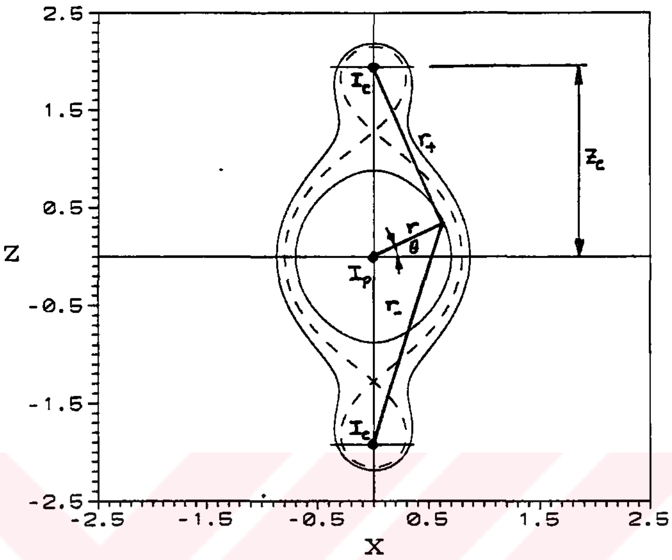

Figure 5.1 Current geometry for three straight wires.

The magnetic field for this unperturbed configuration can be written as follows,

$$\vec{B} = B_0\hat{e}_\phi + \nabla \times \vec{A_\phi} \tag{5.1}$$

where $\vec{A_\phi} = \hat{e}_\phi\Psi(x,z)$ and $\Psi = B_0 L \log(r_+^{2\gamma} r^2 r_-^{2\gamma})$ and $r_\mp^2 = z_c^2 + r^2 \mp 2rz_c\cos\theta$.

For numerical calculations $\gamma = 0.64$; $z_c = 1.93$; the length scale $L = 0.06$ and $R_0 = 2.67$ was chosen [14]. To introduce the effects of nonaxisymmetry into the analysis, $n = 1$ vacuum field perturbation is added to the magnetic field given above, $\delta\vec{B} = \nabla \times \delta\vec{A}$ where $\delta\vec{A} = \hat{e}_z\varepsilon R_0\exp(\frac{x}{R_0})\cos\phi$, $\hat{e}_z$ is parallel to the major axis and ϕ is taken as the toroidal angle.

The field equations are

$$\frac{dx}{d\phi} = \frac{B_x}{B_\phi} \quad ; \quad \frac{dz}{d\phi} = \frac{B_z}{B_\phi} \tag{5.2}$$

and the magnetic field components are,

$$B_x = \frac{\partial \Psi_0}{\partial z} + \varepsilon exp(\frac{x}{R_0})\cos(\phi) \tag{5.3.a}$$

$$B_\phi = \frac{1}{R_0}\left[B_0 - \varepsilon \exp(\frac{x}{R_0})\sin(\phi)\right] \tag{5.3.b}$$

$$B_z = -\frac{\partial \Psi_0}{\partial x} \tag{5.3.c}$$

The magnitude of perturbation is chosen $\frac{\varepsilon}{B_0} = 0.001$. The field lines starting from the vicinity of unperturbed separatrix's X point $(x, z, \phi) = (0.0, 1.28, 0.0)$, are followed 5000 toroidal turns, with 30 values of x_0 chosen at equal intervals between 0.0 and 0.30. Two Poincaré sections were chosen to see the dynamical behaviour of the system. One is placed at a constant toroidal station $\phi = 0$, and the other, at $z = -1.40$ which is a possible location for a divertor plate [14].

Figure 5.2 and 5.3 show the footprints of field lines on the divertor plate and the toriodal station $\phi = 0$; Figure 5.4 and 5.5 are expanded views of lower and upper X points with increasing perturbation amounts, respectively. In the axsymmetric case, the section of smooth toroidal magnetic field surfaces and their destruction to form a stochastic layer can be seen, with the increasing perturbation. Creation and destruction of stability islands placed in chaotic region can also be seen. The changing behaviour of the dynamical system gives a clue about existing bifurcations. In the Figure 5.3, the increasing width of stochastic layer at the midplane with increasing perturbation amounts is seen.

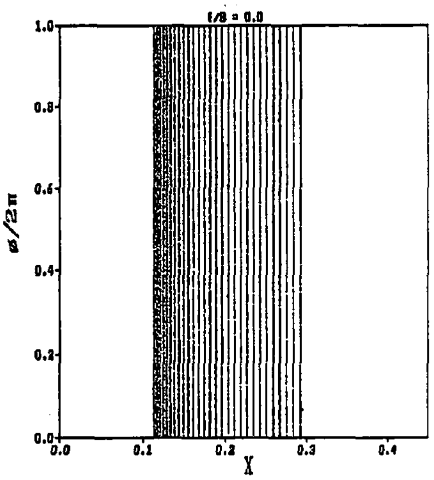

a) ε / B = 0.0000

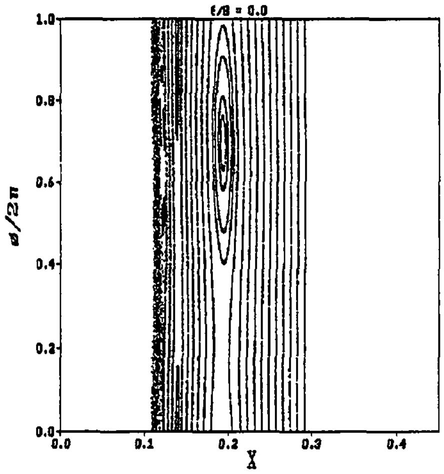

b) ε / B = 0.0001

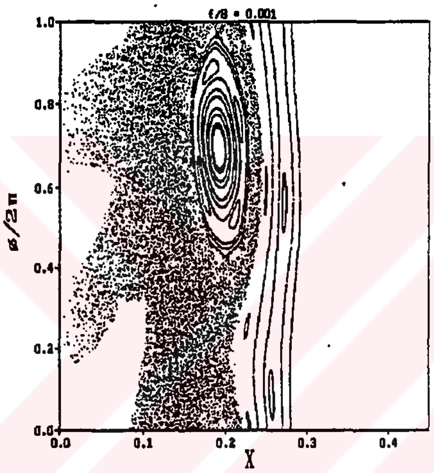

c) ε / B = 0.0010

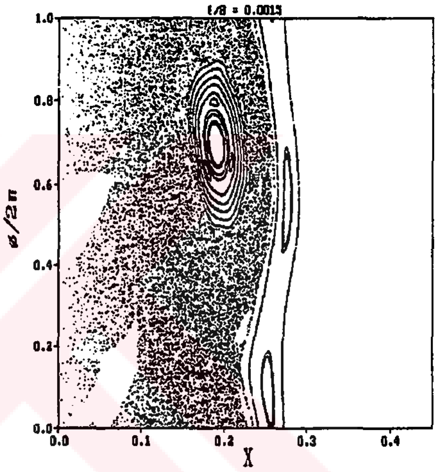

d) ε / B = 0.0015

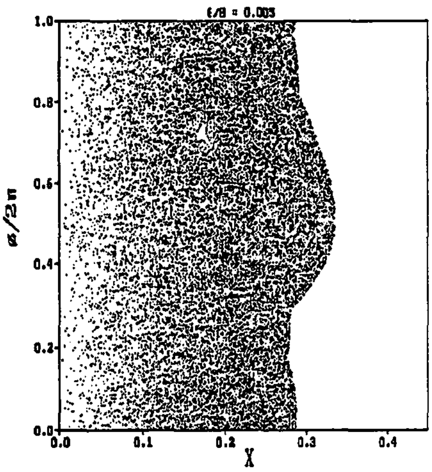

e) ε / B = 0.0050

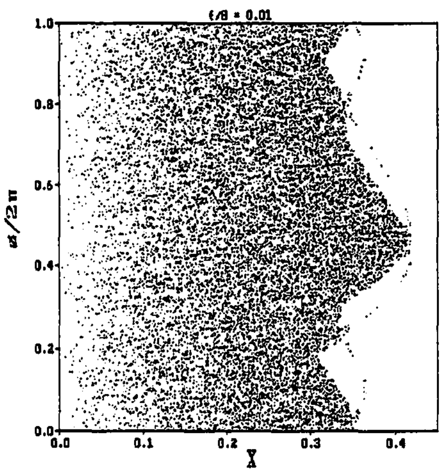

f) ε / B = 0.0100

Figure 5.2 Effect of the different amount of the perturbations on the divertor plate.

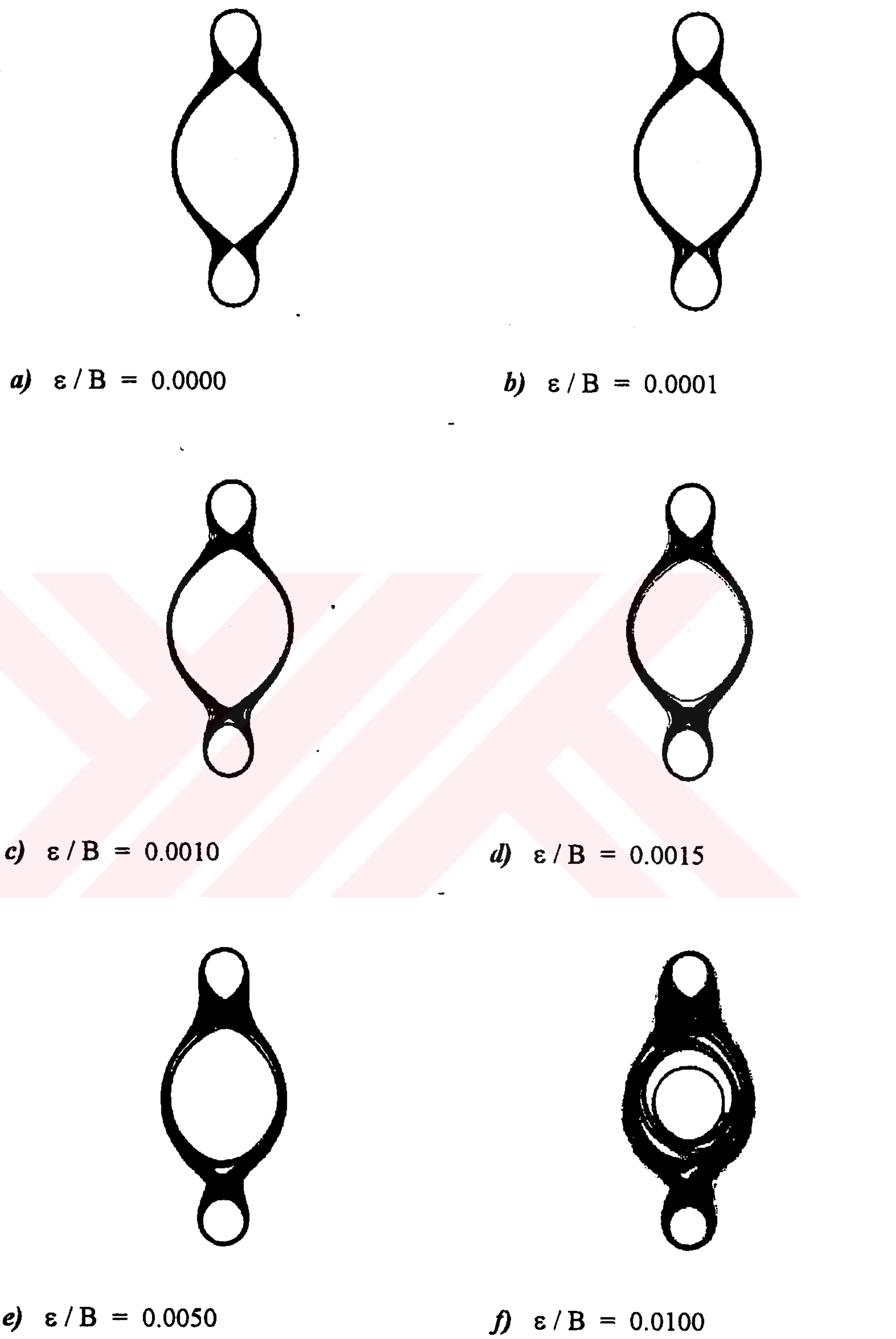

Figure 5.3 Effect of the different amount of perturbations on the toroidal station $\phi = 0.0$.

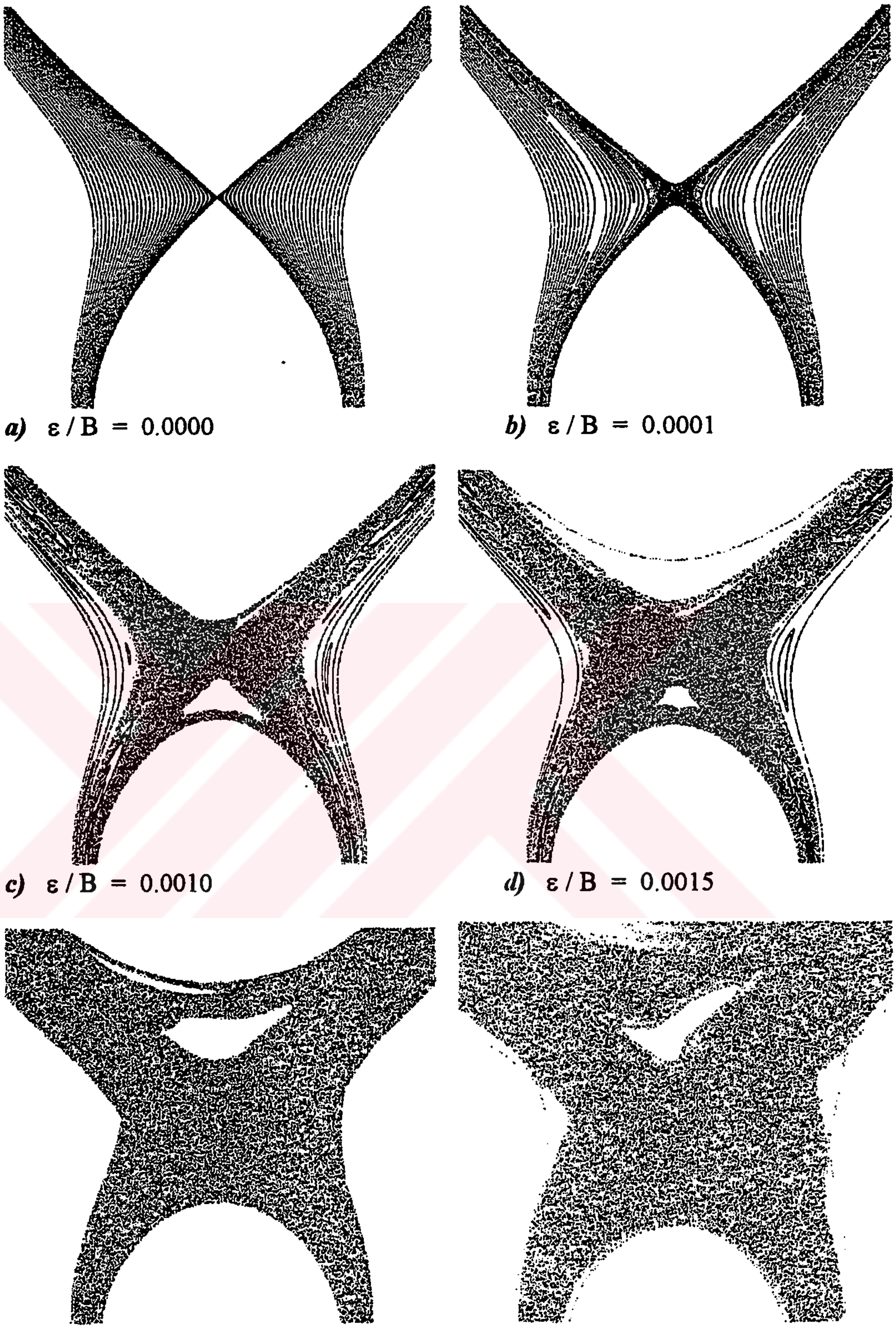

a) $\varepsilon / B = 0.0000$

b) $\varepsilon / B = 0.0001$

c) $\varepsilon / B = 0.0010$

d) $\varepsilon / B = 0.0015$

e) $\varepsilon / B = 0.0050$

f) $\varepsilon / B = 0.0100$

Figure 5.4 Expanded view of the lower X-point

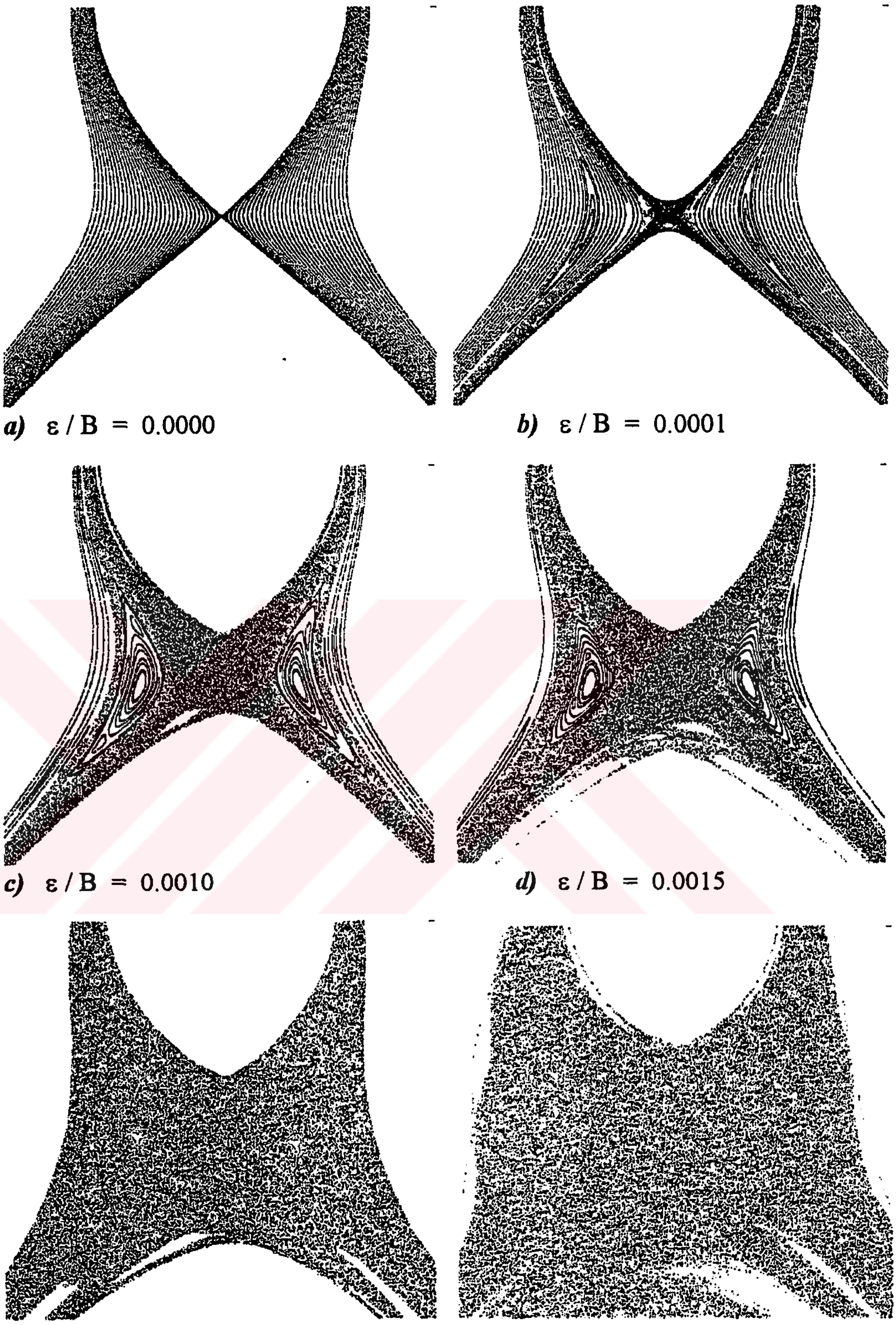

a) ε / B = 0.0000 *b)* ε / B = 0.0001

c) ε / B = 0.0010 *d)* ε / B = 0.0015

e) ε / B = 0.0050 *f)* ε / B = 0.0100

Figure 5.5 Expanded view of the upper X - point

5.2 More Realistic Case

In this subchapter, more realistic case than the one in previous subchapter will be investigated, but the drift motions of particle will again be neglected. Therefore, the magnetic field structure will be taken into account, instead of particle motions. The difference from the previous approach, here, is that the effects of the poloidal field model induced by three coaxial wires (coils) representing the plasma current and the two divertor coils of a tokamak was studied.

In cylindrical coordinates, (R, z, ϕ), the plasma is represented by a coil having radius R_0 and carrying a current of I_p in ϕ direction. Both divertor coils carry currents are defined by two circle $(R_d, \mp z_d, \phi)$ with respect to the plane of the plasma coil, as shown in the Figure 5.6.

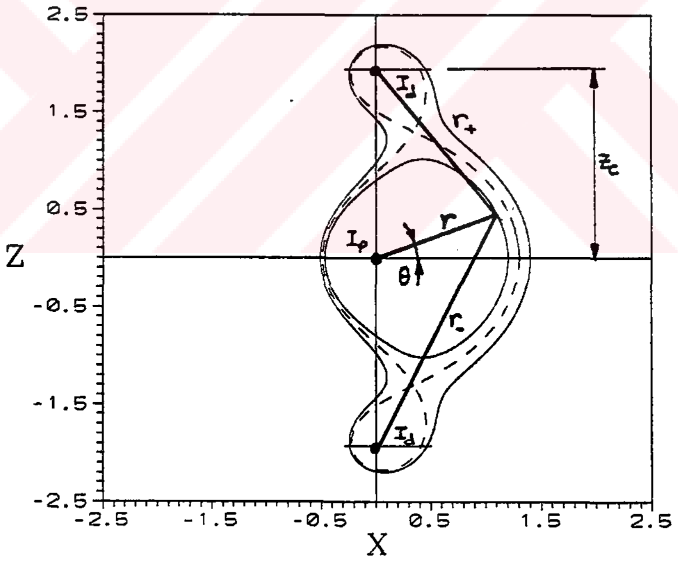

Figure 5.6 Current geometry for three circular wires.

The magnetic field for the unperturbed configuration can be written as

$$\vec{B} = B_0 \frac{\hat{\phi}}{h} + (B_x^p + B_x^+ + B_x^-)\hat{x} + (B_z^p + B_z^+ + B_z^-)\hat{z} \tag{5.4}$$

where $x = R - R_0$, $h = R/R_0 = 1 + (x/R_0)$. The superscript $+$ and $-$ are used to show the field components of the coils placed at $z = +z_d$ and $z = -z_d$, respectively; while superscript p is for that at $z = 0$, i.e., the plasma itself. The magnetic field components are calculated from the following formulae:

$$\begin{aligned} B_x &= I\frac{\mu_0}{4\pi}\frac{2\zeta}{\sqrt{(\rho+\rho_0)^2+\zeta^2}}\left[K(k)+\frac{1-k^2/2}{1-k^2}E(k)\right], \\ B_z &= I\frac{\mu_0}{4\pi}\frac{2}{\sqrt{(\rho+\rho_0)^2+\zeta^2}}\left[K(k)+\frac{\rho_0^2-\rho^2-\zeta^2}{(\rho_0+\rho)^2+\zeta^2}E(k)\right] \end{aligned} \tag{5.5}$$

where

$$k^2 = \frac{4\rho_0\rho}{(\rho_0+\rho)^2+\zeta^2}$$

the poloidal part of the magnetic field is calculated from the vector potential

$$\vec{B} = \nabla \times \vec{A}_\phi$$

where

$$A_\phi = I\frac{\mu_0}{\pi k}\sqrt{\frac{\rho_0}{\rho}}\left[\left(1-\frac{k^2}{2}\right)K(k) - E(k)\right]$$

where K and E are complete elliptic integrals of the first and second kind, respectively.

For B_p :	$I = I_p$;	$\rho_0 = R_0$;	$\rho = R_0 + x$;	$\zeta = z$
For $B_\pm$:	$I = I_d$;	$\rho_0 = R_0 + x_d$;	$\rho = R_0 + x$;	$\zeta = z - (\pm z_d)$

The length scale $\lambda = \dfrac{\mu_0 I_p}{4\pi R_0 B_0} = \dfrac{1}{qR_0}$ where q is the safety factor. The values used for these parameters are

$$x_d = 0\ ; \quad z_d = 1.93\ ; \quad \gamma = I_d/I_p = 0.64\ ; \quad R_0 = 1/\varepsilon\ ; \quad \varepsilon = 0.3\ ; \quad \lambda = 0.06\varepsilon$$

To the above axisymmetric poloidal magnetic field, $n = 1$ vacuum field perturbation terms,

$$\begin{aligned} \delta B_x &= \Theta\lambda B_0 \exp(x/R_0)\cos(\phi) \\ \delta B_\phi &= -\Theta\lambda B_0 \exp(x/R_0)\sin(\phi) \end{aligned} \tag{5.6}$$

are added and $\Theta = 0.001/\lambda$ is chosen.

Figure 5.7 shows the magnetic flux surfaces without perturbation. Every field line starting from the vicinity of X point is followed 2000 toroidal turns. Figure 5.7.a is a toroidal section at $\phi = 0$. Figure 5.7.b is the picture of footprints of field lines on divertor plates and Figure 5.7.c, Figure 5.7.d and Figure 5.8.e are expanded upper X point, lower X point and midplane views of Figure 5.7.a. As seen in the Figure 5.7.a, there are two hyperbolic fixed points. Adding perturbation to this axisymmetric system causes a formation of stochastic layer nearby separatrix as shown in Figure 5.8. In Figure 5.8.b and Figure 5.8.c, a hyperbolic fixed point surrounded by a stochastic region and an elliptical fixed point near the coastline of this stochastic sea can be seen. This gives an idea about an existing bifurcation between the cases of zero and non–zero perturbations. Perhaps not in the hyperbolic fixed point case, but maybe in the stable elliptical fixed point case, one can find the exact coordinates of this point and, moreover, full path of the periodic orbit which passing through that point. One should notice the difference between two phase portraits of straight and circular wires' systems.

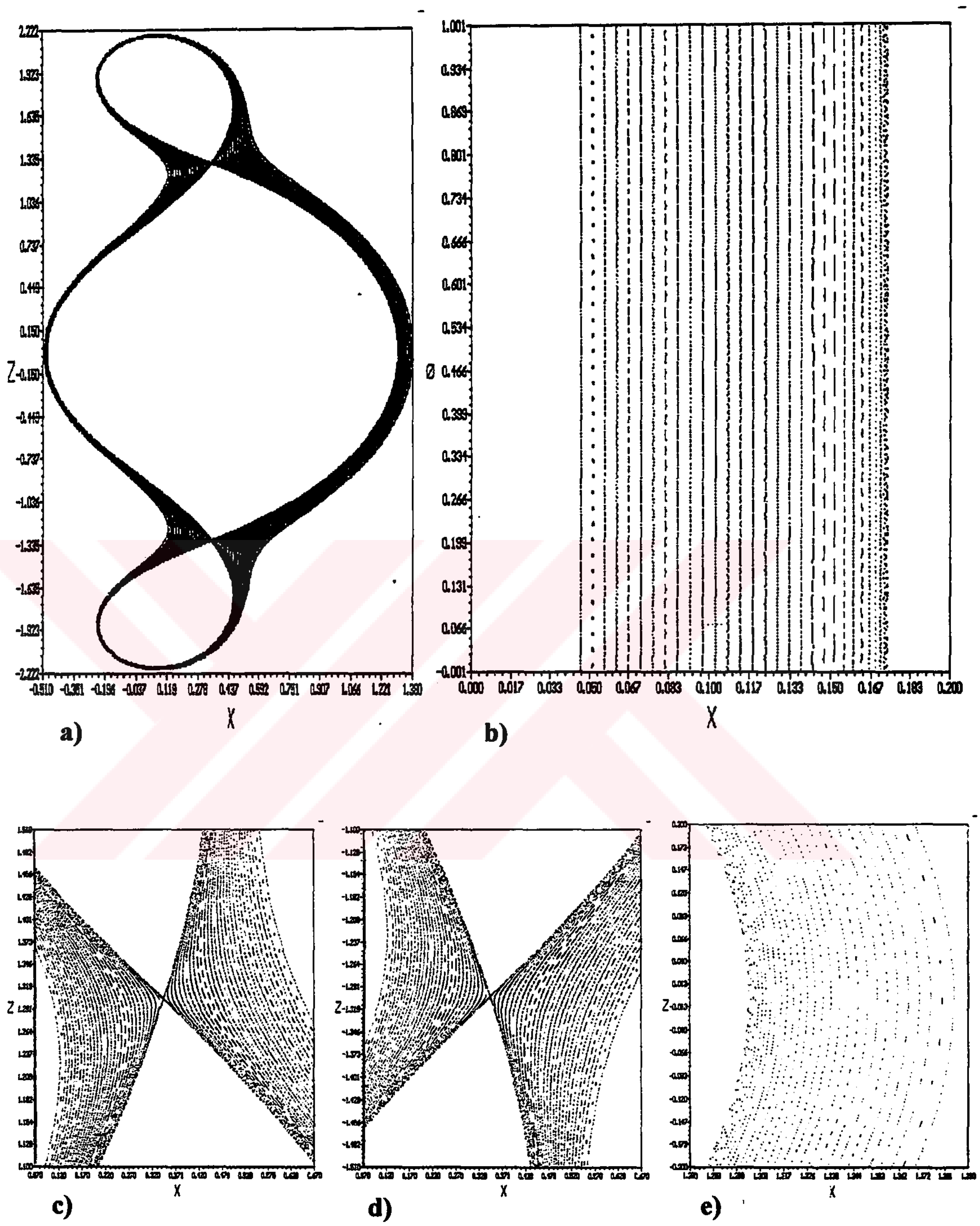

Figure 5.7 Magnetic field structure for circular wires ($\Theta = 0.000/\lambda$).

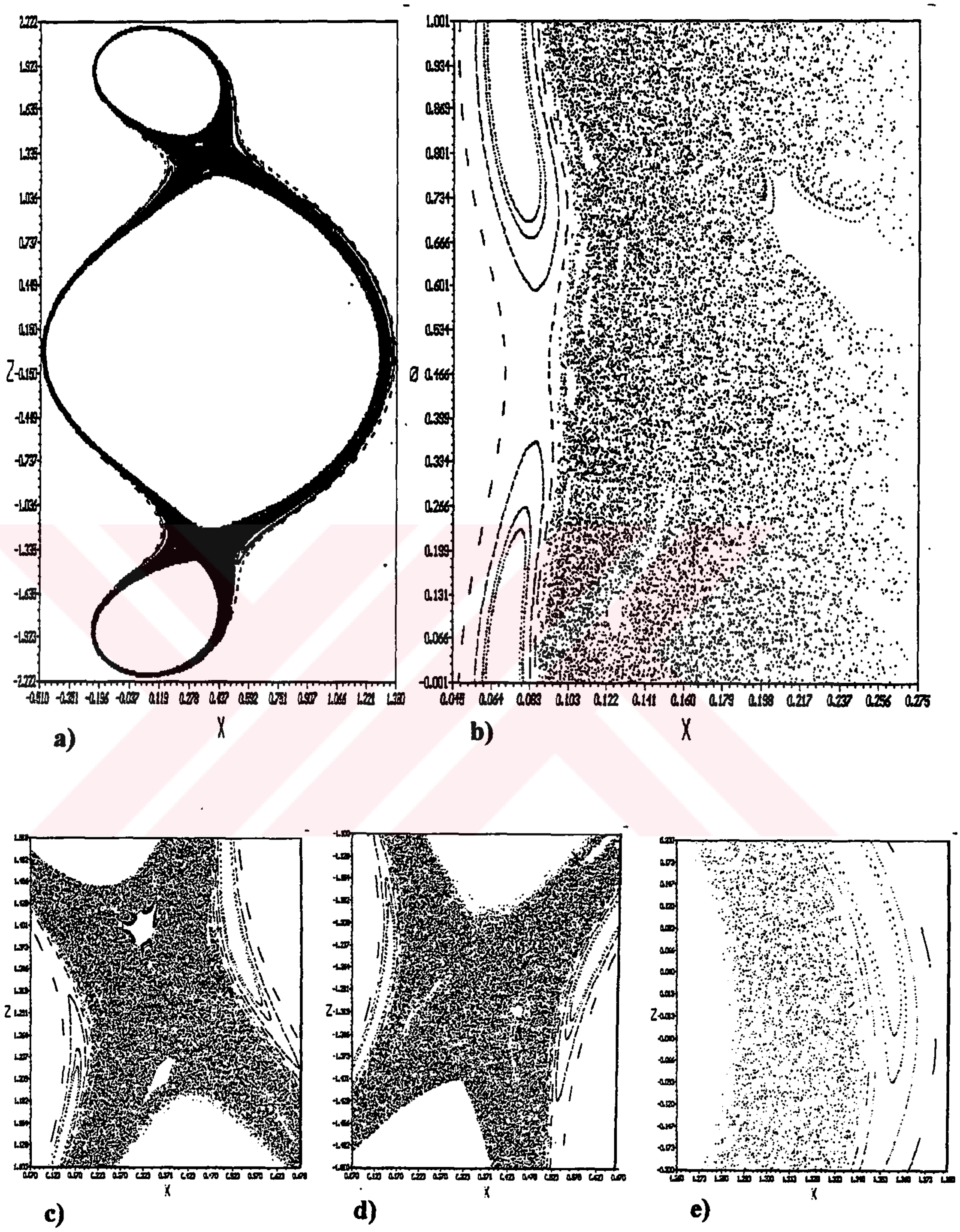

Figure 5.8 Magnetic field structure for circular wires ($\Theta = 0.001/\lambda$).

5.3 True Particle Orbit

The motion of charged particle in a magnetic field can be given as the superposition of a gyration around the guiding center with the cyclotron frequency and the motion of the guiding-center. The integrated equation of motion is the following,

$$\frac{d\vec{x}}{dt} = v_{\parallel}\vec{b} + \frac{\vec{b}}{eB} \times \left[m v_{\parallel}^2 \vec{b} \cdot \nabla \vec{b} + \mu_m \nabla B \right] \tag{5.7}$$

where the magnetic moment is $\mu_m = m v_{\parallel}^2/(2B)$ and $\vec{b} = \vec{B}/B$

As mentioned in the Chapter 3, the total energy ε and the magnetic moment μ_m are the constants of the motion. $\vec{B}(x, z, \phi)$ is normalized by B_0. The magnetic field configuration is created by three circular wires as the one used in Section 5.2.

The autonomous equation system is

$$\frac{dx}{dt} = F_x(x, z, \phi) \ ; \quad \frac{dz}{dt} = F_z(x, z, \phi) \ ; \quad \frac{d\phi}{dt} = F_\phi(x, z, \phi) \ ; \tag{5.8}$$

Figure 5.9.a shows the particle orbit starting from the vicinity of X point (for the stations $x = 0.35, 0.40, 0.45, 0.50, 0.55$ and 0.60; $z = 1.30326$; $\phi = 0.0$) with the $(v_{\parallel}, v_{\perp}) = (0.50, 0.25)$ velocity pair, in the nonperturbed case. Figure 5.9.b shows the same initial conditions except for the velocity pair $(v_{\parallel}, v_{\perp}) = (-0.50, 0.25)$.

Figure 5.9.c and Figure 5.9.d give the drift surfaces for positive and negative parallel velocities, respectively, for zero perturbation. The starting point is X point whose coordinates are $(x = 0.344856, z = 1.30326)$. Figure 5.10 shows the dynamical behaviour of the system with the positive parallel velocity $(v_{\parallel}, v_{\perp}) = (0.50, 0.25)$. Orbits were started at the 20 station for $(0.36 \geq x \leq 0.59;\ z = 1.30326;\ \phi = 0.0)$. Perturbation amplitude was taken as $\Theta = 0.001/\lambda$. The magnetic field's and the particle orbit's dynamical

behaviour in the phase space look like each other, qualitatively, for positive parallel velocity. The effect of direction is important, as one can see in the Figure 5.11. Here, all the initial conditions but $v_{||}$ are taken the same as Figure 5.10. $v_{||} = -0.5$.

Figure 5.12 shows the effects of perturbation on the velocity space $(v_{||}, v_{\perp})$, for the orbits starting inside of the separatrix ($x = 1.26$; $z = 0.0$; $\phi = 0.0$) and outside of the separatrix ($x = 1.35$; $z = 0.0$; $\phi = 0.0$). The number of toroidal turns (not exceeding 200) made by each orbit before it intersects a plate. The sharp boundary in the zero perturbation case becomes smoother for perturbated case, showing the stochastic widening of the boundaries of loss regions. The banana orbits were showed by the character '('.

Figure 5.13 shows the topological character of a stable orbit with non–zero perturbation. The orbit ($x = 0.489$; $z = -1.4$; $\phi = -0.4$; ($v_{||} = -0.95$; $v_{\perp} = 0.81$) lies on a irregular sectioned tube closed on itself after 5 toroidal turns. Pictures indicate the various toroidal stations.

When investigating a dynamical system, the first step is to find, if exists, the fixed points. Then by linearizing the dynamical system around this point, the type of its stability can be found. In the dynamical system considered in this study for the particle motion, if the initial velocities are zero, every point of the whole physical space may be considered as fixed point. Since they are not isolated, it is meaningless to try to find their stability behaviour. This result may be found by thinking the physics of the system. As indicated in the Chapter 3, a magnetic field does not do any work on a charged particle. Thus if a particle is put in a magnetic field with an initial amount of kinetic energy, this energy is conserved along the trajectory. A charged particle in a magnetic field with zero initial velocities will remain at rest. No fixed point can be found with non–zero initial kinetic energy. The next thing to be considered is whether or not a periodical orbit exists. Figure 5.14 shows two different views of a periodic orbit with indicated initial conditions. In this picture, dots represent the possible location of the main plasma body. In 2D Poincaré sections, Figure 5.11, mapping of this orbit is seen to be a center typed one, and to have Lyapunov type but not asymptotical type stability.

Figure 5.15 shows the dynamical behaviour of a trajectory under increasing perturbation amounts. Passage from the coherent structure to chaos is clearly visible.

In order to study the particle motion, we see, in this study, that one should consider true particle equations, although this computation is long and tedious. Because the dynamical behaviour of a particle is quite different than what magnetic field structure can simulate.

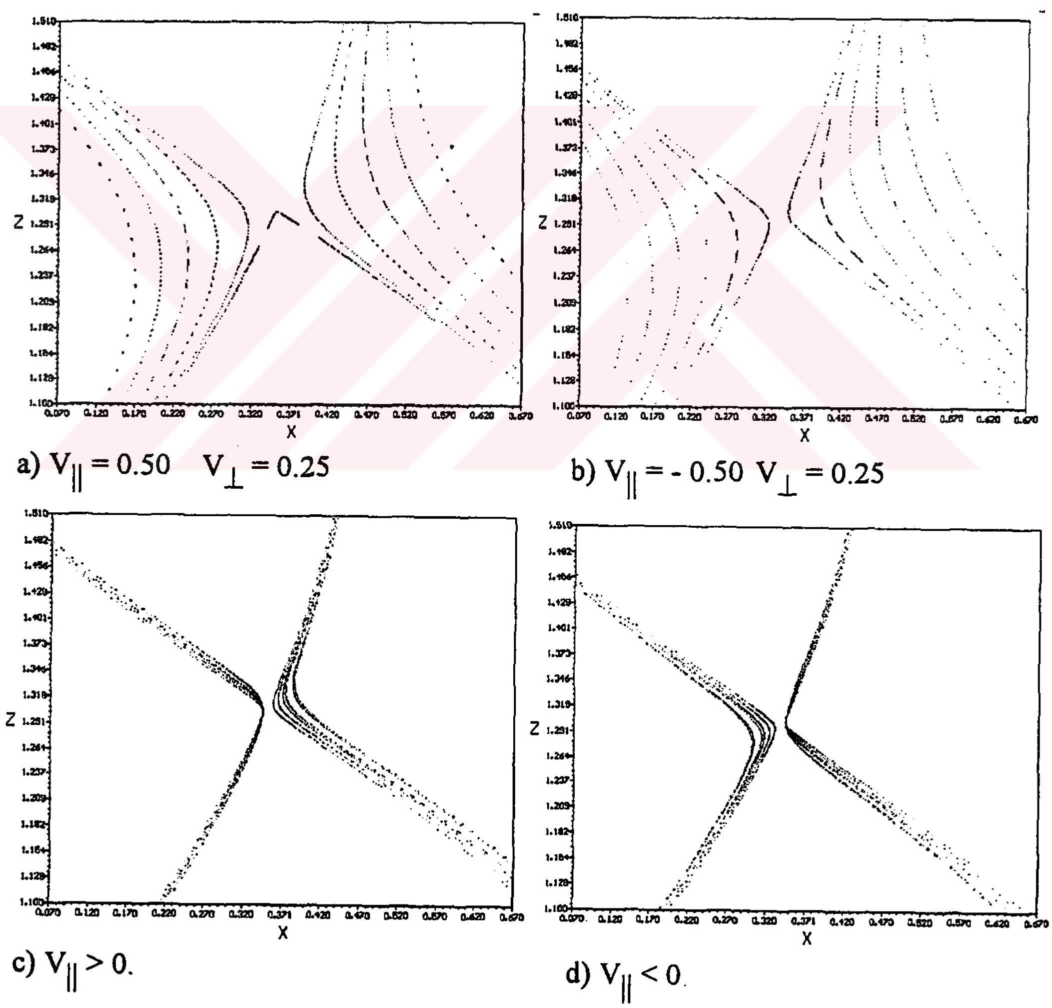

Figure 5.9 Drift surfaces for zero perturbation.

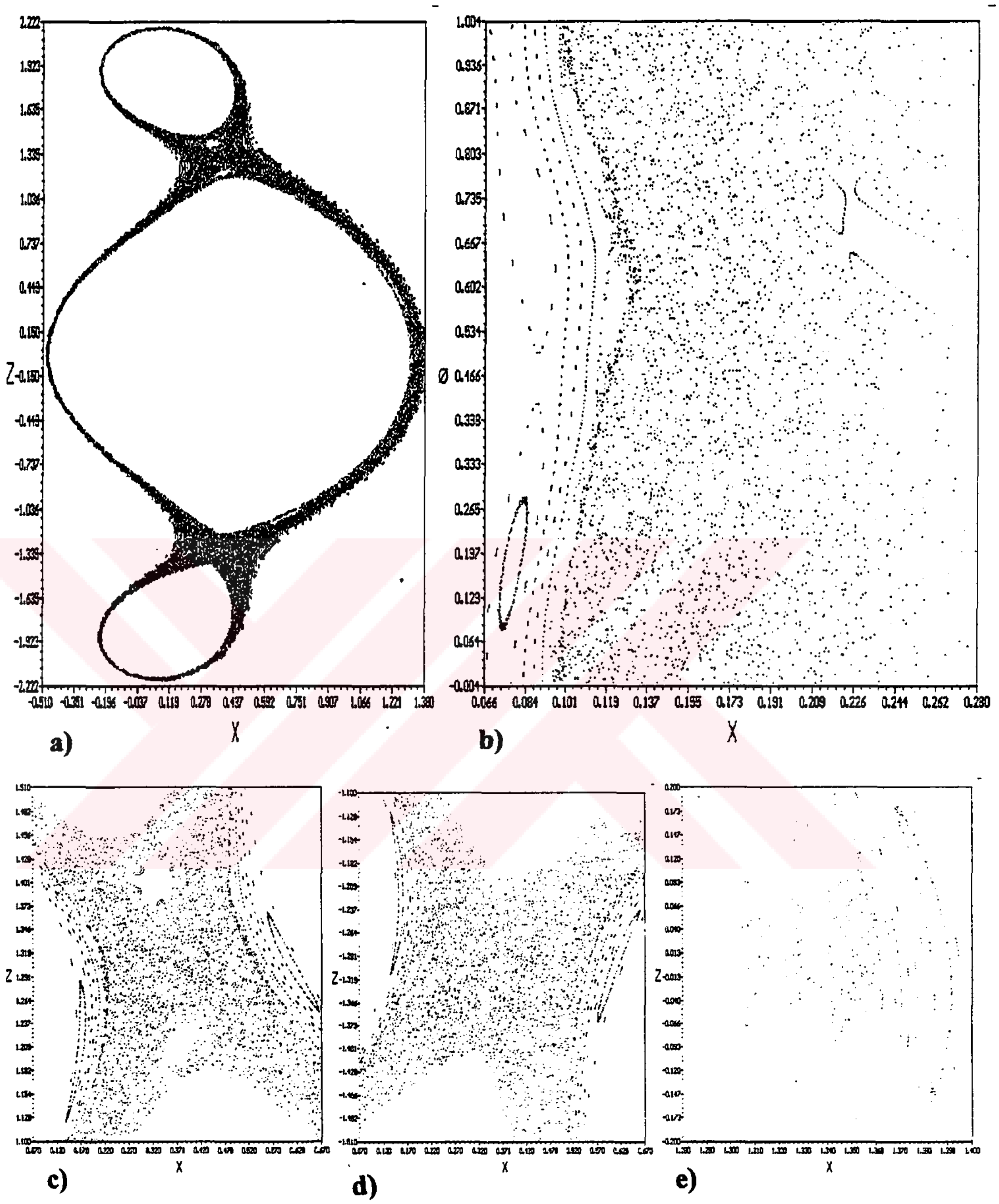

Figure 5.10 Dynamical behaviour of the system, for positive parallel velocities.

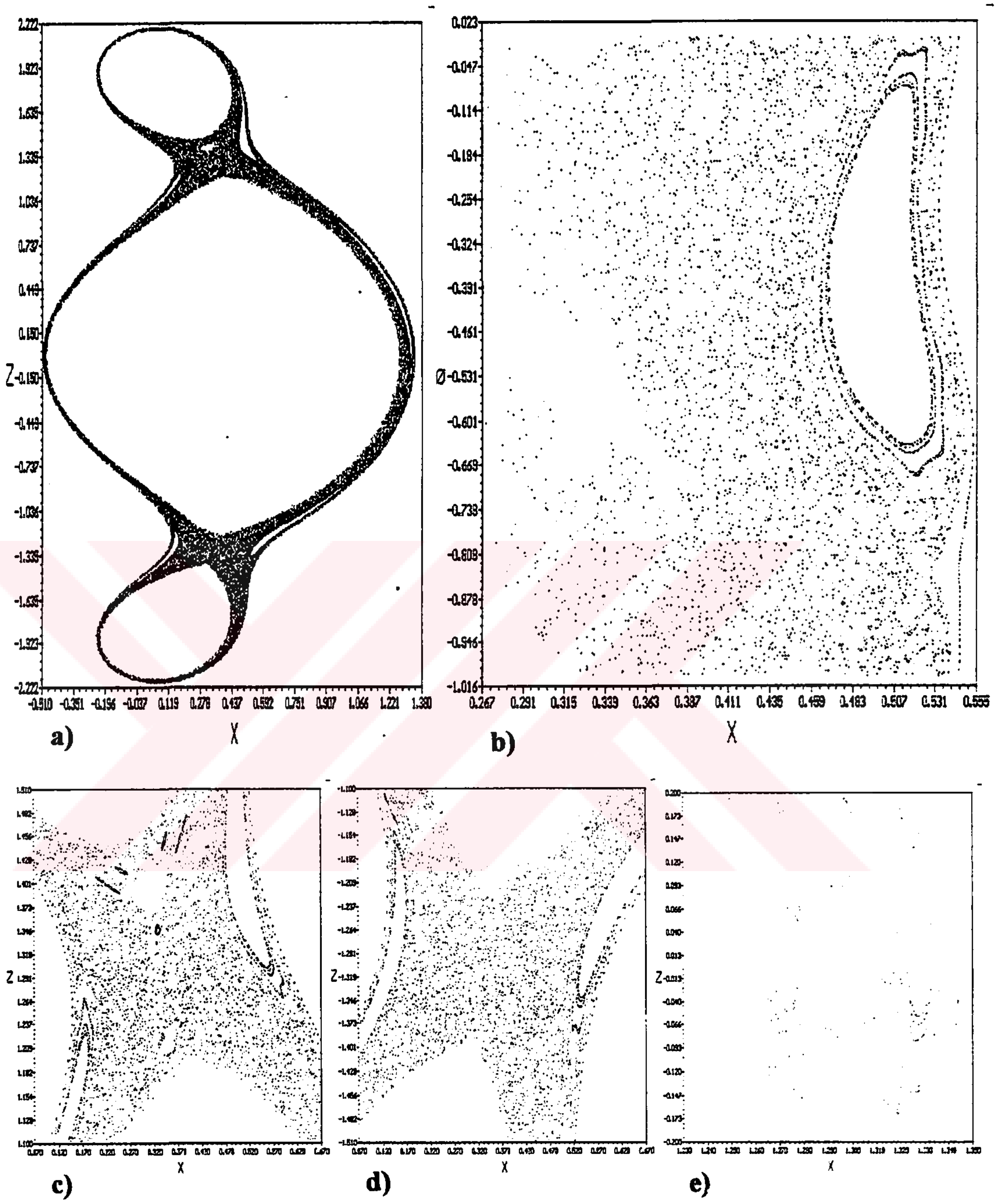

Figure 5.11 Dynamical behaviour of the system, for negative parallel velocities.

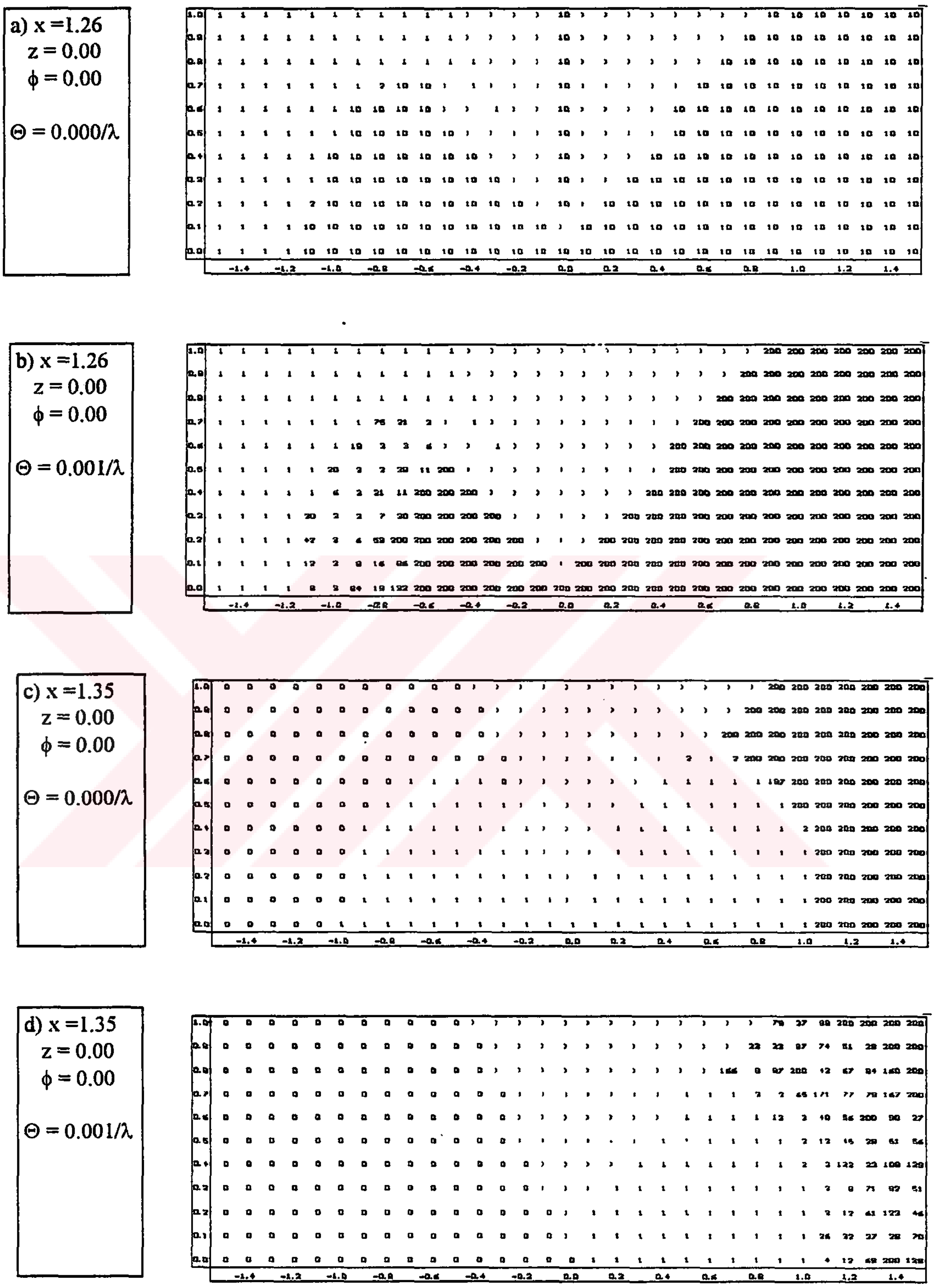

Figure 5.12 Effect of perturbation on velocity space. The vertical axis is $v_\perp$ and the horizontal axis, $v_{||}$. '(' stands for the banana orbits.

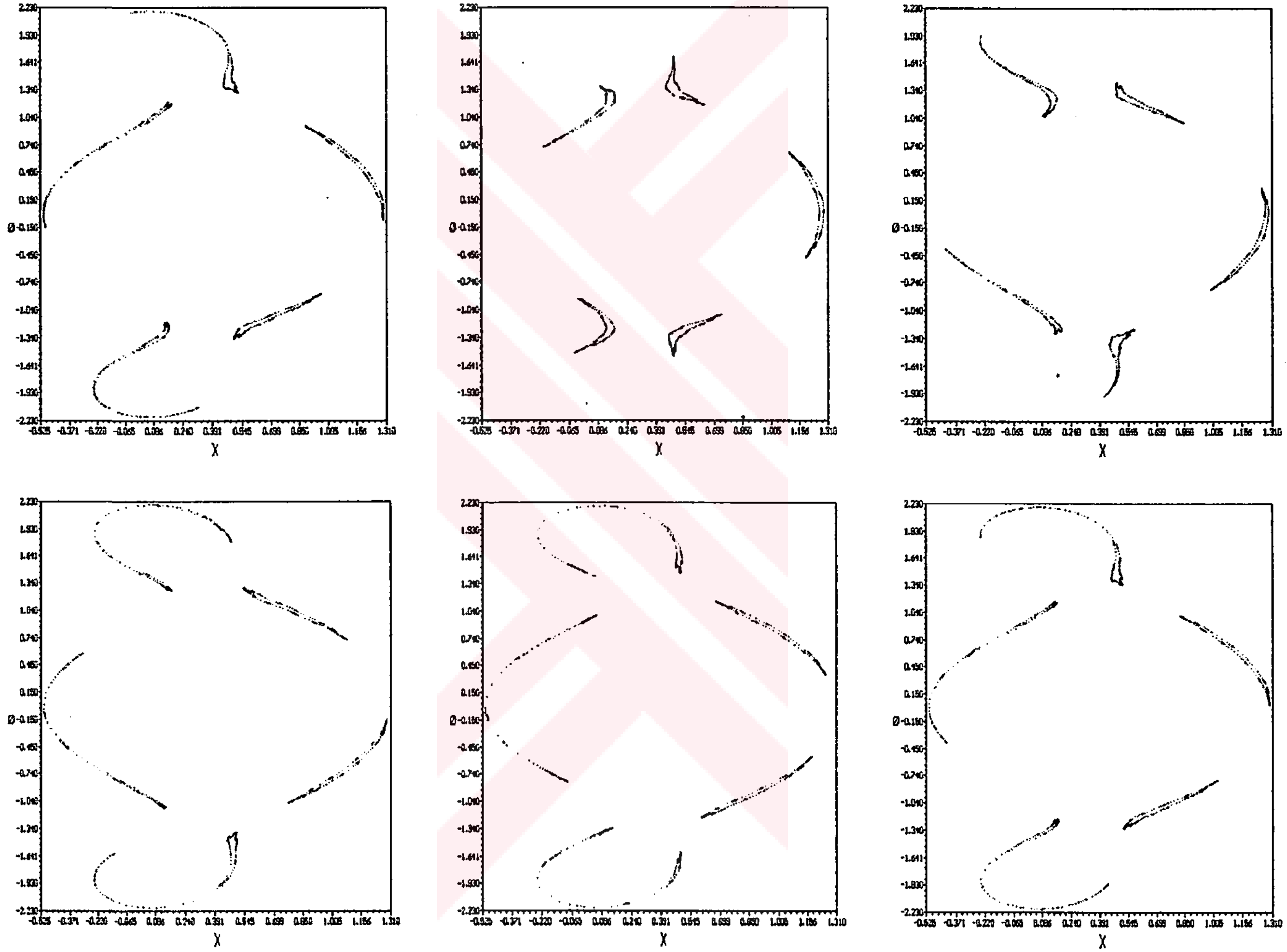

Figure 5.13 Topological structure of a stable orbit with $\Theta = 0.001/\lambda$.

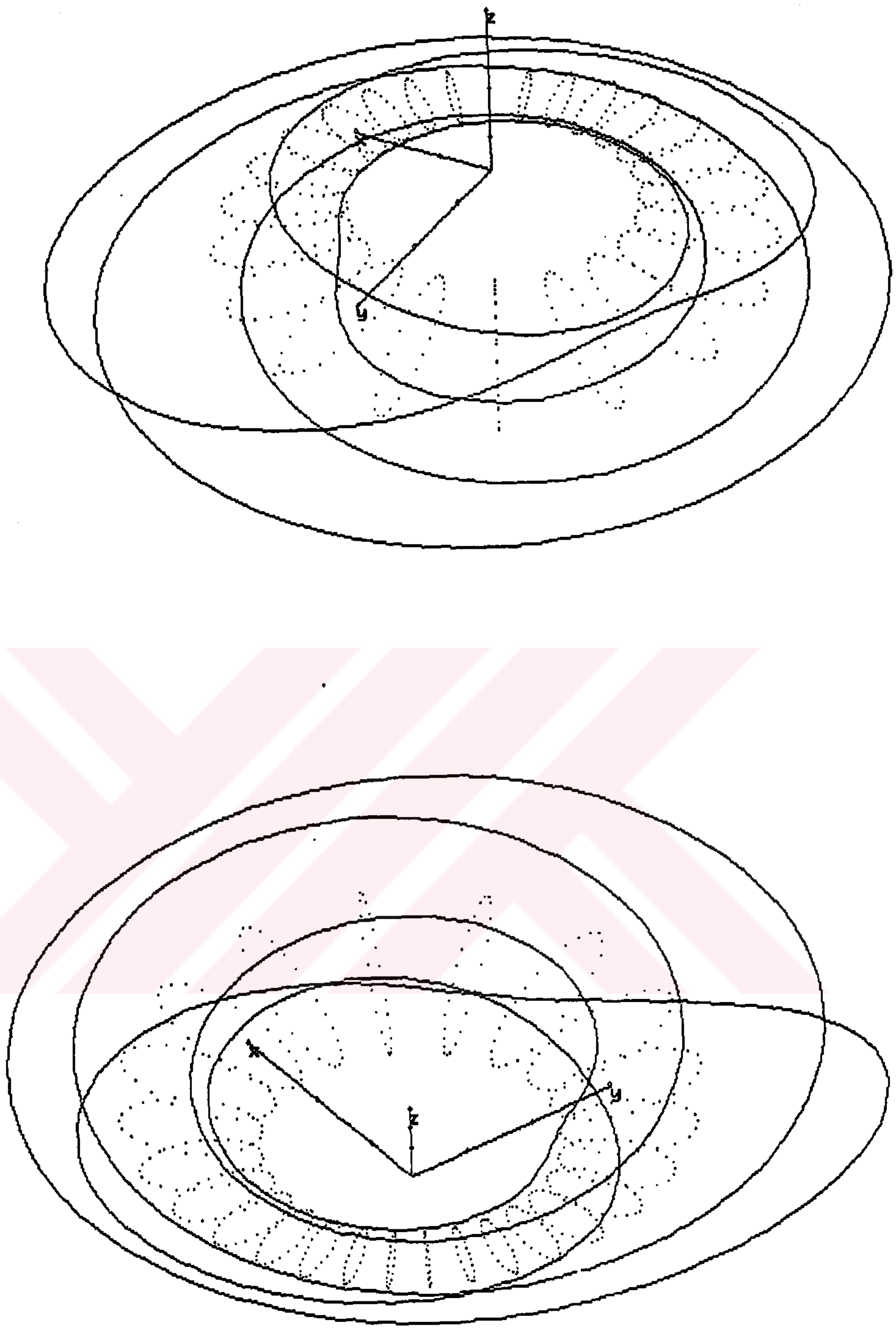

Figure 5.14 Different views of a periodic orbit. ($v_{\|} = -0.5; v_{\perp} = 0.25; x_0 = 0.49064; z_0 = 1.49935; \phi_0 = 0.0$)

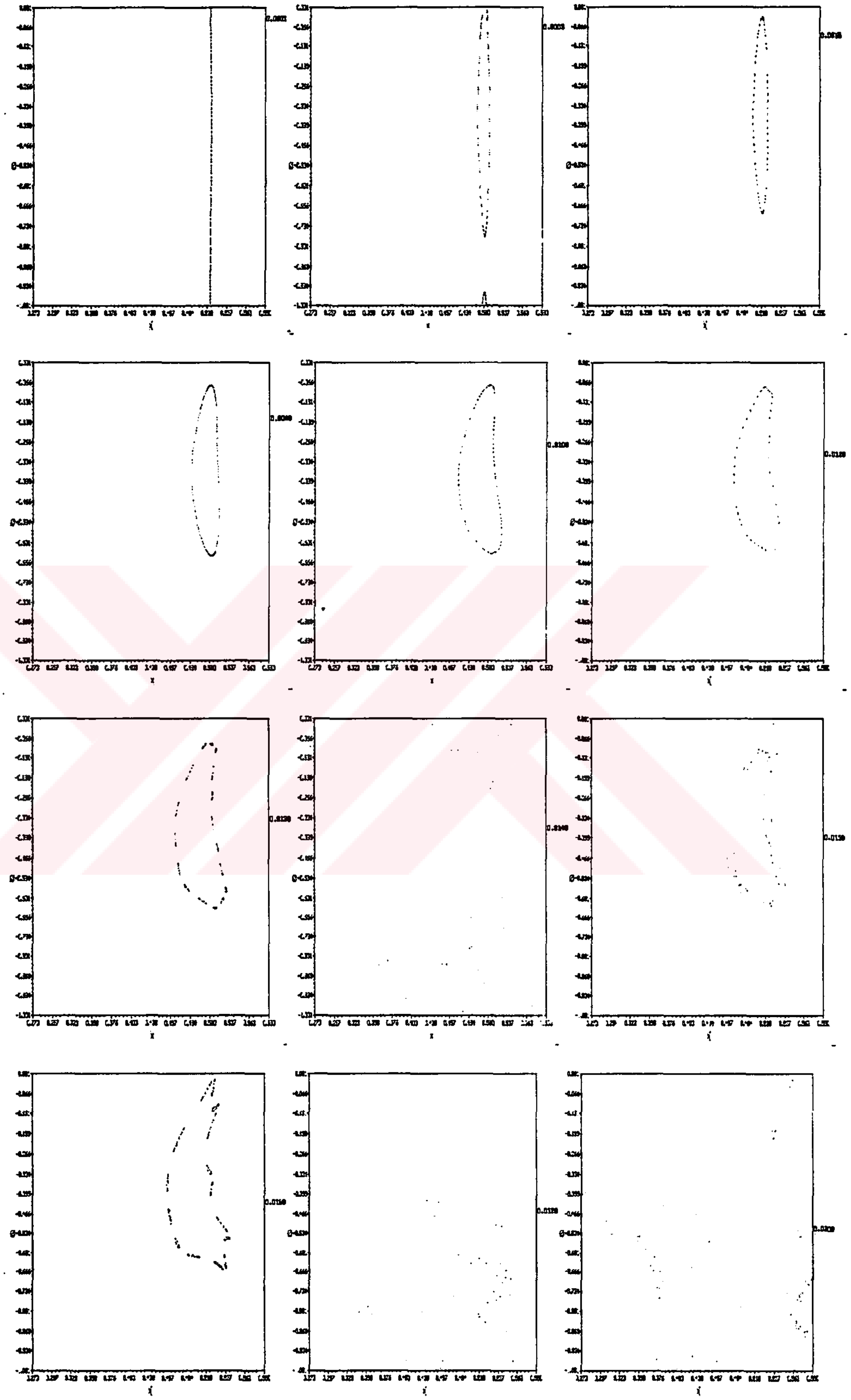

Figure 5.15 Effect of increasing amount of perturbation on a trajectory.

CHAPTER 6

NUMERICAL SCHEME

The ordinary differential equations which governs the motion of the particle are integrated by well–known Adams–Moulton method, after obtaining the necessary four initial values from the Runge–Kutta method. The 4th order Runge–Kutta method is given as following [16],

$$y_{n+1} = y_n + \frac{1}{6}k_1 + \frac{1}{3}k_2 + \frac{1}{3}k_3 + \frac{1}{6}k_4 + O(h^5) \tag{6.1}$$

where,

$$\begin{aligned} k_1 &= hf(x_n, y_n) \quad &;\quad k_2 &= hf\left(x_n + \frac{1}{2}h, y_n + \frac{1}{2}k_1\right) \\ k_3 &= hf\left(x_n + \frac{1}{2}h, y_n + \frac{1}{2}k_2\right) \quad &;\quad k_4 &= hf\left(x_n + h, y_n + k_3\right) \end{aligned}$$

and two step (predictor and corrector steps) of Adams–Moulton method are following respectively [16],

$$\begin{aligned} y_{n+1} &= y_n + \frac{h}{24}(55y_n^{'} - 59y_{n-1}^{'} + 37y_{n-2}^{'} - 9y_{n-3}^{'}) + O(h^5) \\ y_{n+1} &= y_n + \frac{h}{24}(9y_{n+1}^{'} + 19y_n^{'} - 5y_{n-1}^{'} + y_{n-2}^{'}) + O(h^5) \end{aligned} \tag{6.2}$$

When dealing with a problem consisting highly dependence on initial conditions, one needs an almost perfect, if possible, numerical integration. Although there are some non–physical numerical perturbations, such as truncation and round–off errors, these sources of perturbations should never interfere with the physical problem, especially in the problems like the one in this study. The used numerical technique must have proved itself about not producing non–physical results, even after large integration steps. This test may be performed under the zero perturbation condition, i.e., a particle may be taken from one point with a pair of velocity and followed, say 5000 toroidal turns and checked if it still remains on its drift surface or not. But taking zero perturbations cause to drop some terms out in the differential equations and may be source of doubt about the non–zero perturbations case. To be sure about the numerical technique, in this study, a particle whose trajectory stable and lies on a surface with non–zero perturbations were followed 15000 toroidal turns (about 9×10^7 integration steps). Results are presented in Figure 6.1. Figure 6.1.b and 6.1.c shows the blow–up view of the rectangular area of the preceding picture. Here, the importance of the number of digits used in the calculations must be stated. All the computations throughout this study were done for 19 – 20 decimal digits, a property offered by Turbo Pascal 6.0 in extended declaration. To take less had caused some numerical problems.

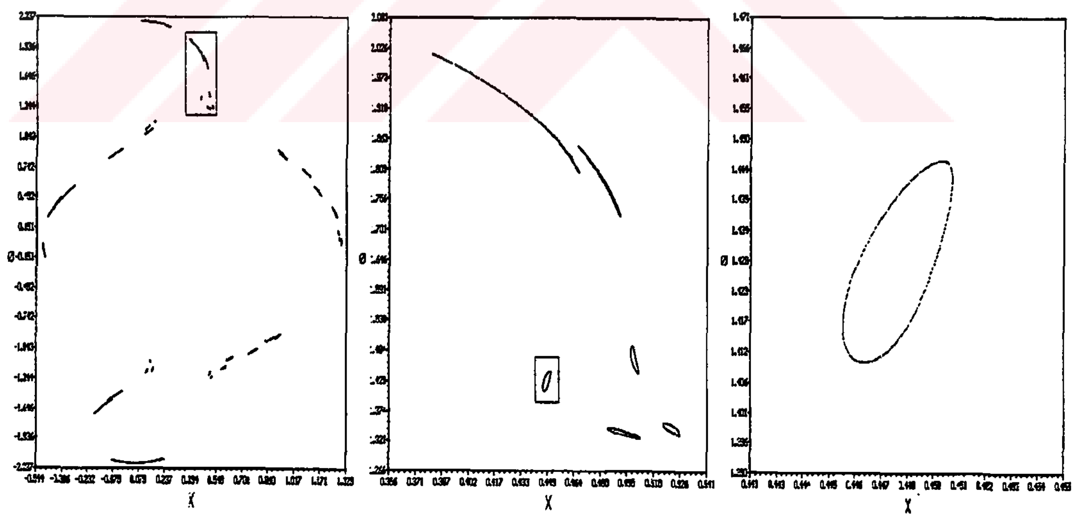

Figure 6.1 Results for 15000 toroidal turns ($\Theta = 0.001/\lambda$).

CHAPTER 7

CONCLUSION

Particle motion in a double–null, poloidal type divertor tokamak was investigated numerically, under following conditions,

i) The velocities were non–relativistic.

ii) Just the ion motions were considered.

iii) Guiding–center approximation was used.

iv) The diffusion effects were neglected.

Chaotic and coherent structures were observed in the phase space of system. The pattern of heat deposition of particles on divertor plates has more complicated structure than suggested before, since the phase space of particles involves more complex structures than that of magnetic field lines. The boundaries of loss cones of particles in velocity space resulting from interception of orbits by divertor plates become gradual transitions due to the chaotic wandering of drift orbits. The used Adams–Moulton integration scheme showed great performance throughout the study.

The next stage of this study will be the investigation of the effect of a transversal electric field on the particle drift orbits. It is hoped to show that an existing electric field plays an important role on the transition between L–mode and H–mode giving better confinement in divertor tokamaks.

REFERENCES

[1] SÄNGER, E., Space Flight, McGraw–Hill, (1965).

[2] MURTHY, S.N.B., FRONING, H.D., Combining Chemical and Electrical–Nuclear Propulsions for High Speed Flight, 10th International Symposium on Air–Breathing Engine, September 1–6, (1991), United Kingdom.

[3] BICKERTON, R.J., The Purpose, Status and Future of Fusion Research, Plasma Physics and Controlled Fusion, Vol 35, Suppl.(12)B, (1993).

[4] CORDEY, J. G., GOLDSTON, R. J., PARKER, R. R., Progress Toward a Tokamak Fusion Reactor, Physics Today, (1992).

[5] CHEN, F. F., Introduction to Plasma Physics, Plenum Press, (1977).

[6] NIU, K., Nuclear Fusion, Cambridge University Press, (1979).

[7] MIYAMOTO, K., Plasma Physics for Nuclear Fusion, MIT press, (1989).

[8] WHITE, R.B., BOOZER, A.H., and HAY, R., Drift Hamiltonian in Magnetic Coordinates, Phys. Fluids 25(3), pp. 575-576, (1982).

[9] WIGGINS, S., Introduction to Applied Nonlinear Dynamical Systems and Chaos, Springer–Verlag, (1990).

[10] KREYSZIG, E., Advanced Engineering Mathematics, John Wiley & Sons, (1979).

[11] ROSS, S.L., Differential Equations, John Wiley & Sons, (1984).

[12] JACKSON, E.A., Perspectives of Nonlinear Dynamics, Vol 1, Cambridge University Press, (1989).

[13] SAGDEEV, R.Z., USIKOV, D.A., ZASLAWSKY, G.M., Nonlinear Physics, Vol 4, Harwood Academic Publishers, (1990).

[14] POMPHREY, N., REIMAN, A., Effect of Nonaxisymmetric Perturbations on the Structure of a Tokamak Poloidal Divertor, Physical Fluids, B4, 938–948, (1992).

[15] PUNJABI, A., VERMA, A., BOOZER, A., Stochastic Broadening of the Separatrix of a Tokamak Divertor, Physical Review Letters, Vol. 69, 3322–3325, (1992).

[16] ABRAMOWITZ, M., STEGUN, I., Handbook of Mathematical Functions, National Bureu of Standards, (1964).

CURRICULUM VITAE

Cuma YARIM was born in Hatay-TÜRKİYE on August 5, 1966. He graduated from The High School of Antakya Kurtuluş, in 1983. He obtained his B.Sc. degree from Istanbul Technical University, Department of Aircraft Engineering, in 1988. After performing his military service, he started his M.Sc education in the Department of Space Science and Technology. He has been working as a research assistant at the faculty since 1992.